

RISA-Net: Rotation-Invariant Structure-Aware Network for Fine-Grained 3D Shape Retrieval

Rao Fu, Jie Yang, Jiawei Sun, Fang-Lue Zhang, Yu-Kun Lai and Lin Gao

Abstract—Fine-grained 3D shape retrieval aims to retrieve 3D shapes similar to a query shape in a repository with models belonging to the same class, which requires shape descriptors to be capable of representing detailed geometric information to discriminate shapes with globally similar structures. Moreover, 3D objects can be placed with arbitrary position and orientation in real-world applications, which further requires shape descriptors to be robust to rigid transformations. The shape descriptions used in existing 3D shape retrieval systems fail to meet the above two criteria. In this paper, we introduce a novel deep architecture, RISA-Net, which learns rotation invariant 3D shape descriptors that are capable of encoding fine-grained geometric information and structural information, and thus achieve accurate results on the task of fine-grained 3D object retrieval. RISA-Net extracts a set of compact and detailed geometric features part-wisely and discriminatively estimates the contribution of each semantic part to shape representation. Furthermore, our method is able to learn the importance of geometric and structural information of all the parts when generating the final compact latent feature of a 3D shape for fine-grained retrieval. We also build and publish a new 3D shape dataset with sub-class labels for validating the performance of fine-grained 3D shape retrieval methods. Qualitative and quantitative experiments show that our RISA-Net outperforms state-of-the-art methods on the fine-grained object retrieval task, demonstrating its capability in geometric detail extraction. The code and dataset are available at: <https://github.com/IGLIC/T/RisaNET>.

Index Terms—3D Shape Retrieval, Fine-grained Retrieval, Rotation-invariant Representation, Convolutional Neural Networks

1 INTRODUCTION

THE recent advances in modeling, digitizing and visualizing 3D physical and virtual objects have led to an explosion in the number of available 3D models on the internet. Therefore, the need for effectively retrieving models from a shape repository has become an important and integral part in the research field of 3D shape analysis. The mainstream shape retrieval methods are content-based approaches, which use shape descriptors to search for similar models. The extraction of shape descriptors with the capability of representing detailed geometric information and global structure is the fundamental task of such approaches. Also, as objects may be placed with arbitrary position and orientation in real-world applications, the requirement on the robustness of the descriptors to rigid transformations increases the difficulty of the problem.

Although existing methods have been proposed to retrieve similar 3D shapes using their shape descriptors, these methods only perform well on coarse-level retrieval, where the shape search engines are asked to retrieve shapes with the same class label among different object classes. These classes normally have radically different overall shapes. Fine-grained object retrieval is more challenging compared

with inter-class retrieval, where the search engine could be asked to find lounge chairs among various sub-classes of chairs, like Barcelona chairs, drafting chairs, slat chairs, etc. Such a fine-grained retrieval task thus requires shape descriptors to be capable of encoding fine-grained properties very well, such as geometric details, because the shapes of different sub-classes in the repository could look similar. Meanwhile, the robustness to rigid transformations, in particular rotations, should be better addressed in the research field of shape retrieval. 3D models in practical applications may not be aligned, but many retrieval methods are not fully invariant to cope with possible rigid transformations. Shape aligning procedures are often required to apply these shape descriptors to 3D shapes with arbitrary rotations, which is not only time consuming, but also less robust.

To tackle the above challenges, we propose a Rotation-Invariant Structure-Aware Network (RISA-Net) for fine-grained 3D shape retrieval which extracts a 3D shape descriptor that is robust to rigid transformation and is also informative to indicate fine-grained shape similarity. Our method is based on the following three observations. Firstly, in both physical object manufacturing and digital 3D shape modeling, assembling interchangeable components or parts has become a practical reality to avoid considerable, and often inconvenient user interactions in 3D object design [1], [2]. It is thus natural to see part-wise differences in 3D models constructed for different functionalities. The parts of an object often vary in importance, and therefore contribute unequally to discriminating different object categories. Therefore, we extract geometric information part-wisely and then use an attention mechanism to learn to weight the contributions of different parts to shape retrieval. Secondly, we need to ensure that the extracted descriptor can well encode the

- R. Fu, J. Yang and L. Gao are with the Beijing Key Laboratory of Mobile Computing and Pervasive Device, Institute of Computing Technology, Chinese Academy of Sciences, Beijing, China and also with University of Chinese Academy of Sciences, Beijing, China.
E-mail: furao17@mails.ucas.ac.cn, {jiayang, lingao}@ict.ac.cn
- J. Sun is with University of Chinese Academy of Science, Beijing, China.
- F. Zhang is with School of Engineering and Computer Science, Victoria University of Wellington, New Zealand.
E-mail:fanglue.zhang@vuw.ac.nz
- Y.-K. Lai is with School of Computer Science and Informatics, Cardiff University, Wales, UK. E-mail:LaiY4@cardiff.ac.uk

Manuscript received September 25, 2020.

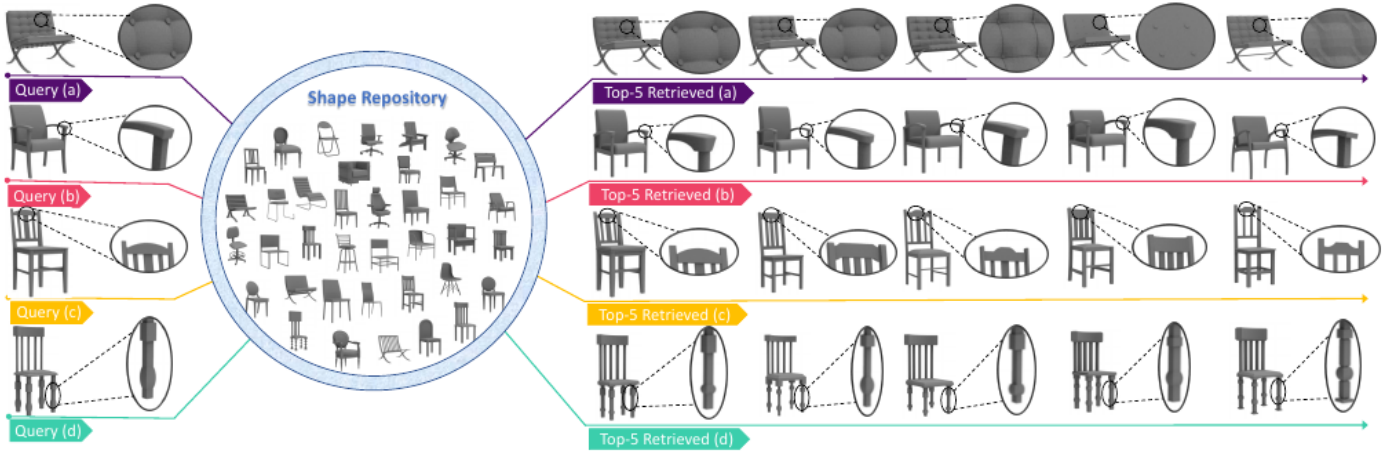


Fig. 1: Four examples of the top-5 retrieval results given query models on the shape dataset with perturbed rotations within the chair category. Our method is able to capture geometric details, learn the importance of each part, and balance the contribution of structure and geometric information in fine-grained retrieval.

subtle difference among the same semantic part of different objects and is invariant to rigid transformations. Intuitively, a latent feature that can be precisely reconstructed to the whole shape must have comprised all detailed geometric information of the original shape. Thus, we propose a variational autoencoder to encode reconstructive rotation-invariant geometric information: edge lengths and dihedral angles. Thirdly, the global structural information is also important in fine-grained object retrieval. Shapes of different sub-classes may share similar local geometry, but their structures could be different. Therefore, we propose a new paradigm to balance the importance of fine-grained geometric information and structural information. In particular, we incorporate the weighted rigid transformation invariant structural information in shape descriptors through fully-connected layers. With the above components, our network is able to learn 3D shape descriptors that achieve a high accuracy when querying shapes with arbitrary poses against the objects of the same class.

In summary, our main contributions are as follows:

- 1) We propose a novel part-based deep model, RISA-Net, which learns fine-grained geometric information part-wisely that is robust to rigid transformation and discriminatively estimates the contribution of each part of the object to shape retrieval. It outperforms the state-of-the-art methods on fine-grained shape retrieval tasks.
- 2) We propose a paradigm that balances structural and geometric information in shape discrimination by learning the weights of structural information and geometric information for the final shape latent feature generation.
- 3) We build and publish a large 3D Shape dataset, RISA-Dataset, to evaluate fine-grained object retrieval methods quantitatively, which provides sub-class labels of all the 8,906 3D shapes.

The following sections are arranged as follows: In Section 2, we briefly summarize the previous works. In Section 3 we elaborate RISA-Net’s structure through its two-

stage feature representation learning and attention mechanism. Section 4.2 includes the fine-grained 3D shape retrieval dataset we constructed, implementation details and experiments to demonstrate the capability of RISA-Net. Finally we conclude our paper and bring up several limitations of our method that could be addressed in the future in Section 5.

2 RELATED WORK

3D shape retrieval is one of the fundamental tasks that discerns the descriptive power of shape representation. In this section, we first review existing research on 3D shape retrieval. Then we look into two-lines of state-of-the-art approaches for 3D shape representation: mesh-based representations and rotation-invariant representations, which are particularly relevant to our work.

2.1 3D Shape Retrieval

Shape retrieval is fundamental to facilitate many applications based on large-scale 3D shape repositories, such as shape modeling [3], template-based deformation [4], and scene modelling [5]. These works retrieve a globally or locally similar shape of the target shape and use it as a component or template for shape modeling, leveraging information provided by the shape repository. The essential component of shape retrieval is effective description of 3D shapes. Among hand-crafted shape descriptors, lightfield descriptors [6] and spherical harmonic descriptors [7] have been used to extract global 3D features, while shape distribution [8], heat kernel diffusion [9], predefined primitives [10] and bag-of-features [11], [12], [13] are able to describe local information for partial shape retrieval, and aggregate local information for global shape retrieval. Recently, facilitated by progresses in deep neural networks, machine learning based methods are adopted to improve the descriptive power of 3D shape representations. Multi-view image-based approaches aim to aggregate features from multi-view images for shape representation, which

aggregates image features through pooling operations [14], image matching [15], [16], or attention-based sequential view aggregation [17], [18]. Instead of projecting shapes to multi-view images, Shi et al. [19] and Steve et al. [20] proposed to project a shape to a cylinder and a unit sphere respectively, and learn features from their projection without extra aggregation operations. Other methods focused on extracting features from point based representations. [21] extracted and aggregated local features from rotation-normalized point sets. [22] transformed the point set into a volumetric representation and introduced a voxel feature encoding layer for feature extraction.

While these methods perform well on large-scale 3D shape retrieval benchmarks [23], [24], their representative power is limited to distinguishing shapes of different subclasses within the same overall class, overlooking fine-grained shape features. Additionally, they focused on only geometric information or spatial information, without discerning the global semantic structure of objects. Observing their drawbacks in sub-class level retrieval, we propose RISA-Net that focuses on fine-grained shape retrieval, which is able to encode both geometric and structural features and weight their importance. We also provide a dataset for quantitatively evaluating fine-grained shape retrieval.

2.2 Mesh-based Representations

There have been numerous studies that investigate how to apply convolution operations on 3D mesh-based models. Masci et al. [25] were the first to extract patches based on local polar coordinates and generalize convolution networks to non-Euclidean manifolds. Sinha et al. [26] used Convolutional Neural Networks (CNNs) to transform a general mesh model into a “geometry image” that encodes local properties of shape surfaces. Anisotropic CNN (ACNN) [27] adopted anisotropic diffusion kernels to construct patches to learn intrinsic correspondences. Monti et al. [28] further improved these ideas by parametrically constructing patch operators through vertex frequency analysis. Alternatively, methods were reported in the literature to perform convolutional operations in the spectral domain. Boscaini et al. [29] used windowed Fourier transform and proposed localized spectral convolutional networks to conduct supervised local feature learning. Xie et al. [30] learned a binary spectral shape descriptor for 3D shape correspondence. Han et al. [31] further proposed a circle convolutional restricted Boltzmann machine (CCRBM) to learn 3D local features in an unsupervised manner. In follow-up work, a mesh convolutional restricted Boltzmann machine was proposed [32], which hierarchically encodes the geometry spatiality of local regions through local function energy distribution of 3D meshes. Hanocka et al. [33] brought up a network with unique convolution and pooling operations on the edges which connect adjacent mesh vertices. Schult et al. [34] proposed a network that applies geodesic and Euclidean convolutional operations in parallel. These methods provide fundamental building blocks for deep learning methods for geometry processing.

A series of recent studies has also indicated the effectiveness of generative models in the literature. The method introduced by Xie et al. [35] is able to encode heat diffusion

based 3D mesh descriptors in a multiscale manner with a set of deep discriminative auto-encoders. More recently, Litany et al. [36] proposed intrinsic Variational Autoencoders (VAEs) for meshes, and applied them to shape completion. A deep model that can learn both geometric and spatial information was successfully established by Han et al. [37]. It learns various types of virtual word features in bag-of-words models and encodes both global and local spatial information simultaneously in an unsupervised way. A recent study by Gao et al. [38] presented a deep generative model for high-quality shape generation through deformable mesh parts and hierarchical VAEs encoding both parts and their structure. Wu et al. [39] proposed using sequence-to-sequence autoencoders to encode shape part-wisely. Inspired by the above works, we propose to use generative models to automatically learn shape descriptors in the latent space.

2.3 Rotation-invariant Representations

Rotation invariance is an important attribute of shape descriptors in real-world applications of 3D shape retrieval. Although studies have been conducted by many researchers, this problem is still insufficiently explored. A common technique in this field is discrete feature aggregation. For instance, the method [21] by Furuya et al. extracted shape descriptors from an oriented point set by aggregating processed local 3D rotation-invariant features. Similarly, Qi et al. [40] sampled multi-orientation 3D input and aggregated them in a multi-orientation volumetric CNN. Some authors have also suggested using multiple images taken from different viewpoints in their deep models. Kanazaki et al. [16] mainly focused on how to aggregate predictions from multiple views and take a single image as input for its prediction. SeqViews2SeqLabels [17] aggregated the sequential views using an encoder-decoder Recurrent Neural Network (RNN) structure with attention. The rotation invariance has been addressed only to a very limited extent because the above methods are not able to deal with arbitrary rotations.

Some recent research works suggested incorporating equivariance directly into the network architecture, because the desired equivalence of transformation can be achieved through constraining the filter structure. Thomas et al. [41] introduced tensor fields to keep translational and rotational equivariance. Worrall et al. [42] used circle harmonics to achieve both translational and 2D rotational equivariance in CNNs. Zhang et al. [43] proposed to represent data by a set of 3D rotations and defined quaternion product units to operate on them.

Another way to achieve equivalence is coordinate transformation. Henriques et al. [44] fixed a sampling grid according to Abelian symmetry. Also, equivariant filter orbit was the main focus of many recent works. Cohen et al. [45] proposed group convolution networks (G-CNNs) with the square rotation group. They provided the evidence for the rotational equivariance of group-convolutions. Worrall et al. [46] proposed CubeNet using Klein’s four-group on 3D voxelized data, which learns interpretable transformations with encoder-decoder networks. They use a 3D rotation equivariant CNN for voxel representations

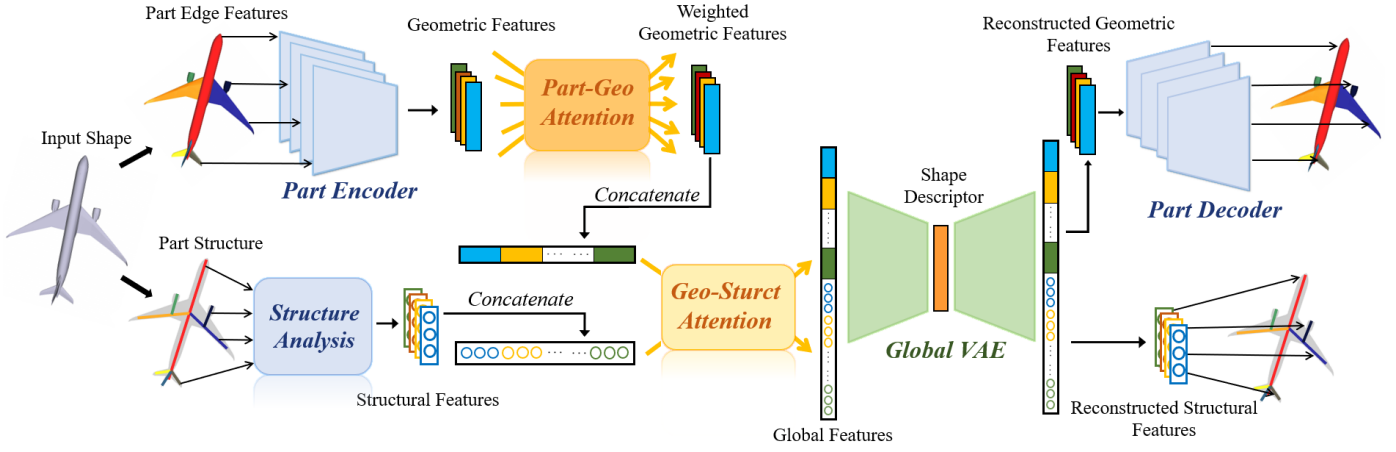


Fig. 2: Pipeline of RISA-Net. From left to the right, i) our method first extracts part-wise base geometric feature and structural feature. ii) Then *PartVAE* encodes base geometric feature to latent space. We then use a part geometry attention mechanism that learns the contribution of each geometric part. iii) Meanwhile, shape structure is analyzed and extracted as structural features. iv) After concatenation, the global geometric feature and structural feature are weighted by a geometry structure attention mechanism. v) The weighted geometric and structural feature are concatenated and then encoded by a *GlobalVAE*, whose latent vector is the high-level shape descriptor of the input object.

with linear equivariance to both translation and right angle rotation. Some previous research works have applied functions on the icosahedron and their convolutions to achieve equivariance on the cyclic group [47] and the icosahedral group [48]. Esteves et al. [20] and Cohen et al. [49] focused on the infinite group $SO(3)$, and used the spherical harmonic transform for the exact implementation of the spherical convolution or correlation. They proposed to first project 3D objects onto a unit sphere and then use spherical convolutional networks to achieve global 3D rotation equivariance. Esteves et al. [20] also defined several $SO(3)$ equivariant operations on spheres to process 3D data, which can achieve better invariance and generalizes well to unseen rotations. The question remains open that how the invariance preservation mechanism can be utilized to learn a shape descriptor for fine-grained shape retrieval.

There are also several recent studies focusing on rotation invariant representations on point clouds, which learn an initial rotation to a canonical pose. Qi et al. [50] adopted an auxiliary alignment network to make model robust to affine transformations by predicting and applying such transformations to input points and features, which was then further improved to handle the variations in point density by [51]. Deng et al. [52] proposed ordering-free point pair features and a deep architecture based on PointNet to encode coordinates to transform-invariant features. But these methods cannot be directly applied to mesh models.

3 RISA-NET

Our method is inspired by the recent progress in the latent vector learning and transformation-invariant feature extraction. To extract 3D shape descriptors with rich geometric details that are robust to rigid transformation, we propose to extract part-wise mesh-based features: edge lengths and dihedral angles. These features preserve rigid transformation invariant and scale-sensitive geometric details, which enable shape reconstruction from these features [53], showing that

complete information is retained. Although these geometric features are descriptive, their high-dimensionality means it would be inefficient to use them directly as shape descriptors. Moreover, these features only describe low-level feature of edges. It thus lacks information of the global semantic structure of the 3D shape. To address these issues, we adopt a set of variational autoencoders (VAEs) with attention mechanism to extract compact features from the base geometric features, which not only retains the translation and rotation invariance of detailed geometric features, but also balances structure and geometric information to a high-level succinct feature for retrieval tasks. In the following subsections, we first symbolize the elements of RISA-Net, and then introduce the components of the network.

3.1 Overview

Fig. 2 illustrates the network architecture of RISA-Net. Given a 3D shape M_i , the input of the network is its semantically segmented parts $\{m_i^p, \forall p \in \{1, 2, \dots, P\}\}$, where P is the number of parts. We extract its base geometric feature f_i^p from each part m_i^p . Then we use a set of *partVAEs* (part-wise variational autoencoders) to encode a geometric feature set $\{f_i^p, \forall p \in [1, P]\}$. Each *partVAE* encodes the geometric feature of the corresponding part edge-wisely to a latent vector z_i^p . Furthermore, we adopt a part-geometry (*Part-Geo*) attention mechanism to weight the importance of each semantic part to amplify the effect of important parts by multiplying the latent vector of each part by the attention weight α^p_i . The weighted latent vector set $\{z_i^p, \forall p \in \{1, 2, \dots, P\}\}$ encodes the geometric information and the contribution of each part to shape discrimination. All the vectors are then concatenated to form a global geometric feature vector g_{v_i} , representing the geometric feature of the whole shape. Similarly, we extract the global structural feature s_{v_i} that is invariant to rigid transformation through part-based structure analysis. As the contributions of geometric and structural features

to fine-grained retrieval vary in different cases, we further learn the importance of geometric and structural features respectively through geometry-structure (*Geo-Struct*) attention mechanism. In particular, we multiply the global geometric feature gv_i and the global structural feature sv_i by the learned geometry weight w_i^g and structure weight w_i^s respectively. Finally, the weighted geometric and structure features are concatenated to get the initial global feature vector fv_i , which is then interpreted as a low-dimensional latent vector zv_i by the global feature variational autoencoder (*GlobalVAE*). zv_i will be used as the shape descriptor of the input 3D shape for the fine-grained retrieval task. Additionally, we append triplet loss term to the original VAE loss to improve the distribution of shape features in the latent space and train our attention mechanisms in an end-to-end manner.

3.2 Geometric Feature Representation

In our observation, globally similar objects could share similar features in some semantic parts, but differ drastically in other parts, since 3D objects are often designed and assembled using different parts to satisfy various desired functions. Therefore, compared with learning features at a low level of granularity for an integrated 3D shape, learning them part-wisely is more effective. In real world applications, 3D objects may be randomly placed, thus are not always strictly aligned or zero-centred to the world coordinate system. Therefore, shape descriptors of 3D objects should be invariant to possible rigid transformations. In case of scaling transformation, the feature needs to be capable of describing the relative size of parts for shape discrimination. For example, comparing a coffee table with a dining table that has the same panel size, the coffee table has shorter legs. Given the above observations, the part-wise geometric feature we extract should be invariant to rotation and translation but sensitive to scaling. Finally, we want the extracted features to contain as much geometric detail as possible, so that the whole 3D shape can be reconstructed from them. Therefore, we represent shapes by edge lengths and dihedral angles, which are reconstructive, scale sensitive and robust to rigid transformations [53].

In particular, the base geometric feature is defined on a set of 3D models that all have the same semantic parts with label $p \in \{1, 2, \dots, P\}$ and E edges with the same connectivity among them, where P and E are the number of Part Semantics and edges respectively. We denote the parts with the same label p of all the models by the set $\{m_i^p, \forall i \in [1, N]\}$, where N is the total number of models. The same topological structure of all the shapes can be utilized to establish part-level correspondences. In our implementation, we use a watertight unit cube mesh with 3075 vertices as the reference model, and perform non-rigid coarse-to-fine registration [54] on the above shape part set, ensuring that all the shapes have the same connectivity as the reference. Each shape m_i^p could be described by its edge lengths and dihedral angles:

$$f_i^p = \left\{ L_i^p, \Theta_i^p \mid L_i^p \in \mathbb{R}_+^E, \Theta_i^p \in [0, 2\pi)^E \right\} \quad (1)$$

where $L_i^p \in \mathbb{R}_+^E$ contains all E edge lengths, and $\Theta_i^p \in [0, 2\pi)^E$ includes dihedral angles of all edges.

The base geometric feature is not ideal for retrieval tasks because of its high dimensionality and redundancy. Therefore, after basic geometric information extraction, feature compression is a necessary step. We propose to use *partVAEs* (part-wise variational autoencoders) to extract high-level features from the base geometric features. Due to its reconstructive property, the high-level latent vector z_i^p learned by *partVAEs* will not only maintain the translation and rotation invariance, but also preserve necessary detailed geometric features for object retrieval.

Fig. 3 illustrates the structure of one *partVAE*. The input of a *partVAE* is an $E \times 2$ dimensional feature vector, f_i^p , containing above basic geometry features. In f_i^p , it concatenates the rows of an $E \times 2$ matrix, where each row corresponds to an edge, and the two columns represent edge lengths and dihedral angles between two adjacent faces. The encoder of *partVAE* learns the posterior distribution between the input data f_i^p and the latent vector z_i^p . As the encoder learns local geometric features, convolutional operations on undirected edges are required. Thus, we adapt *MeshConv* operation [33] to encode our reconstructive base geometric feature. In particular, the input is filtered by the first three convolutional layers, where the convolutional operation on the i^{th} edge e_i is defined as:

$$y_i = W_e * x_i + W_{n_{e,1}} * \frac{\sum_{j \in N_{e_{i,1}}} x_j}{|N_{e_{i,1}}|} + W_{n_{e,2}} * \frac{\sum_{j \in N_{e_{i,2}}} x_j}{|N_{e_{i,2}}|} + b_e \quad (2)$$

where $x_i \in \mathbb{R}^2$ is the feature (edge length and dihedral angle) of edge e_i . Edges are treated as unidirectional, and each mesh part is registered from a unit cube, which is a closed, manifold mesh. Therefore, e_i is adjacent to two faces. Within each adjacent face of e_i , in the counter-clockwise order, we refer to the edge immediately after e_i as the first adjacent edge, and the edge immediately after the first adjacent edge as the second adjacent edge. Denote by $N_{e_{i,1}}$ and $N_{e_{i,2}}$ the sets of first and second adjacent edges of e_i , respectively. In our case, as each edge has 4 neighboring edges, the numbers of elements in each set $|N_{e_{i,1}}| = |N_{e_{i,2}}| = 2$. $W_e, W_{n_{e,1}}, W_{n_{e,2}} \in \mathbb{R}^{2 \times 2}$ are learnable weights of convolutional operations on an edge and its adjacent edges. $b_e \in \mathbb{R}^2$ is the bias term. Additionally, all convolutional layers are appended with a batch-norm layer and a Leaky-ReLU layer with the slope for negative input $\tilde{\alpha} = 0.02$.

The output of three consecutive convolutional layers is fed into two fully-connected layers to obtain its mean and variance respectively, where the mean z_i^p is the latent vector of *partVAE*. After that, the decoder learns to reconstruct f_i^p from the latent vector z_i^p , the network structure of which is symmetric with the encoder without sharing weights. Each *partVAE* is able to extract high-level latent feature of a semantic part, thus depicts geometric information part-wisely. We assume that the number of parts is fixed for all the objects in the same class. However, not all parts need to be present on a given shape. If an input model misses some parts, the input for the corresponding *partVAEs* will be zero-matrices, and the latent vectors of these parts are set as zeros.

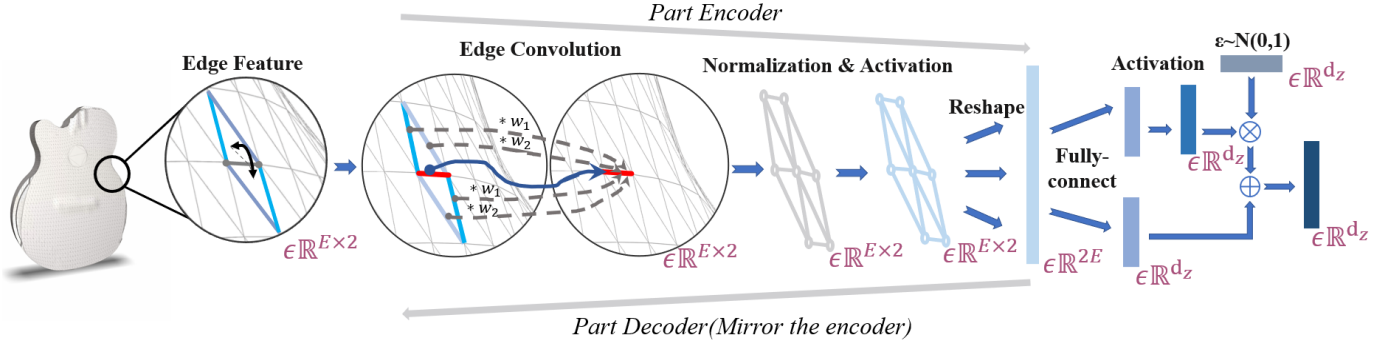


Fig. 3: The structure of one partVAE. PartVAE encodes edge features through convolutional operations on edges and their adjacent edges. E denotes the number of edges of a mesh model. d_z denotes the dimension of the latent vector of PartVAE

3.3 Part Geometry Attention Mechanism

Each semantic part does not contribute equally in shape representation. For example, when measuring the similarity of two car models, car bodies may be more important than car mirrors. Therefore, we further introduce a *Part-Geo* (part geometry) attention mechanism to learn to determine the importance of each part of each shape in fine-grained retrieval.

We define an attention vector $\alpha_i = [\alpha_i^1, \alpha_i^2, \dots, \alpha_i^P]$ to denote the importance of each part for object M_i . The higher the value of α_i^p , the more discriminative the part p is when recognizing shapes. Following [55], the attention vector α_i is obtained by softmax of the dot-products of key vector K_i and query vector Q_i :

$$\alpha_i = \text{softmax}(K_i^T \cdot Q_i) \quad (3)$$

where $K_i = [K_i^{(1)}, K_i^{(2)}, \dots, K_i^{(P)}]$ represents the key feature of the part i , which is a linear transformation of its latent vector: $K_i^p = W_K^p z_i^p$. The query vector Q_i is the summation of the linear transformation of the latent features of all parts: $Q_i = \sum_p W_Q^p z_i^p$. Here, $W_K^p, W_Q^p \in \mathbb{R}^{d_h \times d_z}$, d_z is the dimension of the latent vector, and d_h is the dimension of the key and query features. The attention vector is jointly trained with other parts of the neural network.

Thus, the output of the *Part-Geo* attention mechanism is a set of weighted geometric features, $\{\alpha_i^1 z_i^1, \alpha_i^2 z_i^2, \dots, \alpha_i^P z_i^P\}$, which are concatenated and reshaped to a vector $gv_i \in \mathbb{R}^{P \times d_z}$, representing the global geometric information of the object.

3.4 Structural Information Representation

Despite the importance of structural information in shape representation, it has been neglected by existing methods for shape retrieval. Visually similar shapes often share similar structure. Objects that have parts with similar geometric features can be distinguishable when their structures are highly different. Therefore, we incorporate the global structure of an object as part of our representation.

We represent the structural information by the spatial relationships among the semantic parts. Same as geometric features, the proposed structural features are also robust to rigid transformation. For each class of 3D objects, we

first define one semantic part as the body part that all models must contain. If there are more than one common semantic parts in all models, we select the part with the largest average volume. We observe that the existence of non-body parts and their relative positions to the body part are important for shape discrimination, which can be used to interpret structural information of shapes. As shown in Fig. 2, we describe the structure of objects by an 11-dimensional vector sv_i , defined as follows:

- $sv_1 \in \{0, 1\}$ denotes whether the part exists in the input 3D shape.
- $sv_2 \in \mathbb{R}$ denotes the distance from the center of the current part to the center of the body part.
- $[sv_3, sv_4, sv_5] \in [-1, 1]^3$ denotes the cosine of the angles between the first principal component of the current part and the first three principal components of the body part respectively.
- $[sv_6, sv_7, sv_8] \in [-1, 1]^3$ denotes the cosine of the angles between the second principal component of the current part and the first three principal component of the body part respectively.
- $[sv_9, sv_{10}, sv_{11}] \in \mathbb{R}^3$ denotes the unit direction from the center of the body part to the center of the current part.

3.5 Geometry-Structure Attention Mechanism

Although the objects of the same class all share similar structures, objects belonging to different classes have different diversity in the composition. For example, all guitars share the same structure, but chairs have diverse compositions. Thus geometric information and structural information could have different contribution when discriminating objects belonging to different classes. Therefore, the extracted compact global geometric and structural features gv_i and sv_i need to be re-weighted to balance their contributions to the final shape representation. To achieve this, we introduce a *Geo-Struct* (geometry and structure) attention mechanism to learn to balance the importance of structure and geometric information in shape representation. We define a score vector $w_i = [w_i^g, w_i^s] \in [0, 1]^2$ for model M_i , representing the weights of geometric and structural information. The

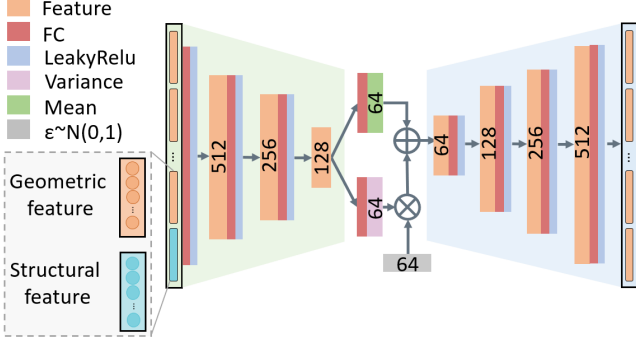


Fig. 4: Network architecture of globalVAE. GlobalVAE encodes part geometric features and global structural feature through three consecutive fully-connected layers. The latent vector is the shape descriptor of input shape.

score vector is learned through two fully-connected sub-networks:

$$w_i = \text{softmax}([F(gv_i), G(sv_i)]) \quad (4)$$

where $F : \mathbb{R}^{d_z} \rightarrow [0, 1]$ and $G : \mathbb{R}^{11} \rightarrow [0, 1]$. In implementation, $F(\cdot)$ contains two fully-connected layers, and the dimension of output vectors of the two layers are 32 and 1 respectively. $G(\cdot)$ contains two fully-connected layers as well, where the dimension of output vectors are 16 and 1 respectively. The global geometric feature and structural features are multiplied by their corresponding weight scores respectively and then concatenated to form the global feature: $fv_i \in \mathbb{R}^{P \times (d_z + 11)}$, which contains weighted geometric and structural information of the object.

3.6 Global Feature Encoding

To encode both geometric and structural feature into one latent space, we further use a *GlobalVAE* (global feature variational autoencoder) to encode global geometric and structural information into a reconstructive compact representation. We use the architecture of globalVAE illustrated in Fig. 4. The *GlobalVAE* comprises three fully-connected layers, each appended with a leaky Relu layer with the slope of negative input $\tilde{\alpha} = 0.02$. The structure of *GlobalVAE* ensures that its latent vector zv_i contains the geometric information of all parts as well as the global structural information.

3.7 Losses

To optimize the network parameters of our model, we adopt three loss-terms that enable a discriminative latent space for fine-grained shape retrieval.

VAE Losses. Our optimization objective function includes a Kullback–Leibler (KL) divergence term and a reconstruction term for each *partVAE* and the *GlobalVAE*. The KL divergence term regularizes the latent space, while the reconstruction term ensures that the input features can be explained by our autoencoders. Therefore, the loss function for all the *partVAEs* includes the KL divergence terms and the terms measuring the differences between all the input base geometric features and their decoding results:

$$L_{VAE}^{part} = \frac{1}{P_i} \sum_{p=1}^{P_i} (f_i^p - f_i'^p)^2 + \gamma \sum_{p=1}^{P_i} D_{KL}^p(q(z_i^p | f_i'^p) \| p(z_i^p)) \quad (5)$$

where P_i is the number of the parts of model M_i , f_i^p is the base feature of the the p^{th} part, $f_i'^p$ is the reconstructed feature of the p^{th} part. In the second term, γ is a weight that balances both terms, $p(z_i^p)$ is the prior probability distribution, $q(z_i^p | f_i'^p)$ denotes the posterior probability, and D_{KL}^p denotes the KL divergence of the p^{th} partVAE. γ is a constant, which is set as 1×10^5 in our experiments. We define the loss for the *GlobalVAE* in a similar way.

Triplet Losses. Using above losses for VAEs, the distribution of the latent vectors is able to cluster the models of the repository in the feature space to some extent. However, it can be further optimized by minimizing the distance between the features of similar shapes and enforcing a margin between dissimilar shapes. Besides, we use a triplet loss [56] to optimize the final feature distribution in the latent space, which also helps the attention mechanisms to find the distinguished parts and balance the importance of structure information.

For the globalVAE, we define the term as:

$$L_{triplet}^{global} = \sum_i [D(zv_i^a, zv_i^p) - D(zv_i^a, zv_i^n) + \eta]_+ \quad (6)$$

where zv_i^a , zv_i^p and zv_i^n are the latent features of an anchor model (i.e., a chosen model in the training iteration), a positive model (i.e., a model of the same sub-class as the anchor model) and a negative model (i.e., a model of a different sub-class from the anchor model). $D(\cdot, \cdot)$ is a measure of distance between two vectors in the latent space. We use the Euclidean distance $D(v_1, v_2) = \|v_1 - v_2\|_2^2$ in our experiments. η is the threshold of the margin between the distances from the reference model to the similar and dissimilar models. In implementation, the Euclidean distance $D(\cdot, \cdot)$ between features are normalized to $[0, 1]$ in each batch. We set η to 0.3 in the following experiments.

For the set of *partVAEs*, we define a triplet loss term as:

$$L_{triplet}^{part} = \sum_i [D(gv_i^a, gv_i^p) - D(gv_i^a, gv_i^n) + \eta]_+ \quad (7)$$

We use the term to refine the distribution of the global geometric feature gv_i for the entire set of *partVAEs*.

Overall Loss. The overall loss of RISA-Net is:

$$L = L_{VAE}^{part} + \lambda_1 L_{VAE}^{global} + \lambda_2 L_{triplet}^{part} + \lambda_3 L_{triplet}^{global} \quad (8)$$

where λ_1 , λ_2 and λ_3 are hyper-parameters to balance the weights of different loss terms, which are defaultly set as 1×10^3 , 1×10^2 , and 1×10^2 in our all experiments.

3.8 Model Training and Shape Retrieval

We feed 3D shapes of all the sub-classes of the same class to RISA-Net to learn to encode base features into a latent feature for that class. The *partVAE* set with *Part-Geo* attention mechanism first learns a high-level geometric feature set from base geometric features, using the reconstruction loss,

KL losses and triplet losses. At the same time, the high-level geometric feature set is balanced with structural feature and then fed to the *GlobalVAE* to learn to generate the final latent feature vector, where we minimize the same three types of loss terms during training. In addition, we use the objects of the same sub-class as similar shapes and objects of different sub-classes as dissimilar shapes when minimizing the triplet losses.

For an input 3D object M_i , we use the latent vector of the *GlobalVAE* gv_i as its shape descriptor. For each query shape, we rank the shapes in the repository according to the Euclidean distance between their shape descriptors. Note that the distance metric used in retrieval is the same as in the triplet loss, which is the Euclidean distance.

4 EXPERIMENTAL RESULTS

In this section, we describe our dataset, implementation details and the experiments to validate the effectiveness of RISA-Net. We build a RISA-dataset with 3D shapes labeled at the sub-class level to support experiments of fine-grained retrieval and provide both quantitative and qualitative comparisons between RISA-Net and other state-of-the-art methods. We also show shape retrieval results on other publicly available datasets to demonstrate the generalizability of the shape descriptors extracted by our RISA-Net. Finally, we conduct ablation studies to verify the necessity and complementarity of all the components of our model.

4.1 Dataset

Retrieving a model against shapes within the same class but belonging to different sub-classes is a typical fine-grained shape retrieval task, where the repository contains globally similar shapes that differ in some details. Most of the existing large-scale 3D object datasets are annotated with only class level labels, which is not suitable for fine-grained retrieval task. For example, ModelNet [57] contains 662 object categories but only a few of them are given sub-class labels. Part of ShapeNet models [58] also have intra-class semantic labels, but the labeling precision and amount are not sufficient to test intra-class retrieval methods. Although FRGC v2 dataset [59] is labeled with an intra-class manner, the dataset only focuses on facial recognition rather than common objects retrieval. Therefore, we build a new dataset with sub-class level annotations, designed for training, evaluating and comparing fine-grained shape retrieval methods, which is used to demonstrate the effectiveness of our latent descriptor for fine-grained shape retrieval. It could be used to support and evaluate future research on fine-grained 3D shape classification and retrieval task. The shapes used in our fine-grained 3D object retrieval dataset is a subset of SDM-NET data [38], containing 8,906 3D models from six object categories. The six categories are knife, guitar, car, plane, chair and table, which are further grouped into 175 sub-classes. Each sub-class of models is annotated with semantic labels, which are defined by their distinguishable features compared with other sub-classes, such as functionality, product model number and style. Take the category of guitar as an example, objects are further

categorized into twelve sub-classes including double-neck guitar, acoustic, cutaway, Flying V, Gibson Explore, Gibson Les Paul, etc. These semantic labels are assigned according to their style and standard model number.

All of the intra-class labels were annotated manually. For clarification, the original annotation from ShapeNet is used as a reference for our annotators. Additionally, some unrealistic shapes that are hard to be categorized were discarded, because keeping them would confuse the retrieval method by using ambiguous sub-class labels, leading to inaccurate quantitative analysis. Please refer to our supplementary materials for more detailed information of the dataset.

4.2 Implementation Details

4.2.1 Dataset Preparation

We evaluated the performance of RISA-Net in the fine-grained 3D object retrieval task on the RISA-Dataset introduced in the previous subsection. We tested the performance of RISA-Net on all the six object categories. To demonstrate the robustness of RISA-Net to rigid transformation, we perturbed all models in the dataset by transforming each model with a random rotation in $SO(3)$. All experiments were conducted on the perturbed dataset.

4.2.2 Training Details

The experiments were carried out on a machine with an Intel i7-6850 CPU, 128GB RAM and a GTX 1080Ti GPU. We randomly split the dataset into training and testing sets with a ratio of 4:1. The network is trained in an end-to-end manner. In optimization, we adopt Adam Optimizer [60] and set the learning rate to constant 1×10^{-5} . The batch size of each iteration is 8. The optimization repeats until the loss converges.

TABLE 1: Comparison of average performance on six categories with different dimensions of latent vectors.

(d_z, d_s)	(32, 32)	(32, 64)	(32, 128)
mAP(micro, macro)	(0.53,0.44)	(0.49,0.36)	(0.49,0.39)
(d_z, d_s)	(64, 32)	(64, 64)	(64, 128)
mAP(micro, macro)	(0.59,0.51)	(0.61,0.51)	(0.22,0.15)
(d_z, d_s)	(128, 32)	(128, 64)	(128, 128)
mAP(micro, macro)	(0.55,0.47)	(0.57,0.49)	(0.49,0.38)

4.2.3 Parameter Setting

We adopt the same network structure and hyper-parameters on all six object categories. *GlobalVAE* comprises 3 fully-connected layers, the dimensions of which are set to 512, 256, and 128 respectively. We evaluated the mean average precision (mAP) of the retrieval results on the six object categories with different dimensions of the latent vectors of *PartVAE* and *GlobalVAE*, and find that 64 dimensional latent vectors are the most empirically effective settings for both of them. The experimental results on different latent vector settings are illustrated in Table 1, where d_z and d_s denote dimensions of the latent vectors of partVAE and globalVAE respectively.

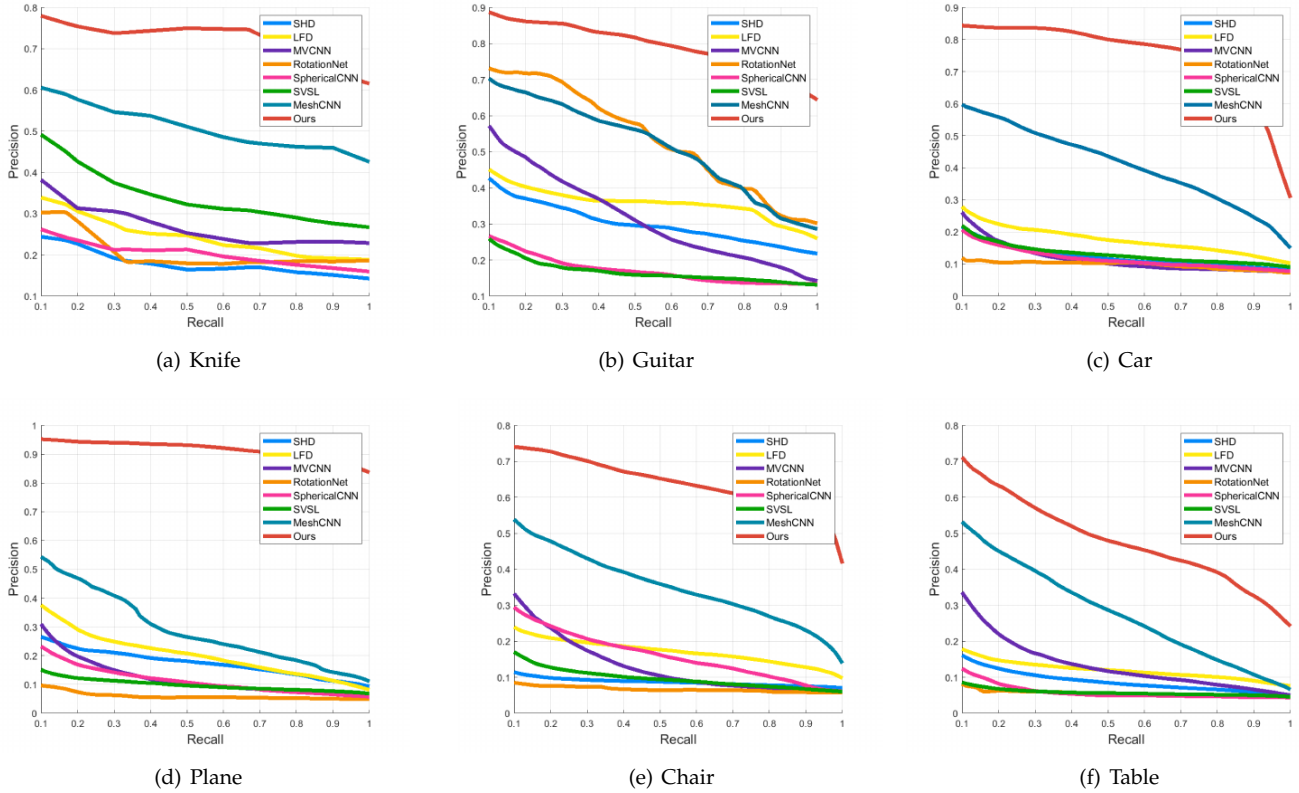


Fig. 5: Comparison of Precision-Recall Curves of different methods on six object categories.

TABLE 2: Comparison between RISA-Net and other methods using five metrics on six object categories. The reported results are based on the test set for fairness.

Methods	micro					macro				
	NN	FT	ST	NDCG	mAP	NN	FT	ST	NDCG	mAP
SHD [7]	0.1620	0.1335	0.2450	0.4358	0.1617	0.0904	0.0748	0.1461	0.3516	0.1107
LFD [6]	0.2241	0.1827	0.3134	0.4860	0.2143	0.1277	0.1065	0.1929	0.4010	0.1525
MVCNN [14]	0.3374	0.1680	0.2682	0.4864	0.1884	0.2324	0.1223	0.1874	0.4123	0.1492
RotationNet [41]	0.1688	0.1385	0.2301	0.4339	0.1717	0.1211	0.0989	0.1515	0.3634	0.1349
Spherical [20]	0.1590	0.1195	0.2068	0.4233	0.1404	0.1002	0.0781	0.1289	0.3551	0.1061
SVSL [17]	0.1604	0.1318	0.2381	0.4573	0.1541	0.0956	0.0832	0.1422	0.3769	0.1095
MeshCNN [33]	0.4653	0.2979	0.4561	0.6739	0.2938	0.3541	0.2421	0.3815	0.5760	0.2448
Ours	0.7378	0.5670	0.6892	0.7878	0.6125	0.6003	0.4642	0.5631	0.7065	0.5142

4.3 Fine-Grained Shape Retrieval

In the fine-grained object retrieval task, we query a shape among the shapes of the same class in the dataset. As mentioned above, all shapes are perturbed by random rotations in the experiment. RISA-Net is trained to extract latent feature vectors for shape representation, which are then used to measure the similarity between the query and all the shapes of the same class. The similarity between shapes is measured by the Euclidean distance between shape descriptors. If a retrieved shape is in the same sub-class with the query shape, we denote it as a successful retrieval. Fig. 1 shows the top five retrieved results for four query shapes on chair category. Since RISA-Net is able to find shapes with matched geometric details, it performs well in the sub-class retrieval. Specifically, as shown in the first row of Fig. 1, RISA-Net captures that the query object has grid cotton pad on the chair back, and then retrieves shapes with similar features. Meanwhile, the retrieved results with lower rankings also

show the capability of RISA-Net. As shown in the last row, the query shape has a slat back and turned legs. RISA-Net successfully retrieves shapes with matched features, which are in the same sub-class as the query shape. For more retrieval results, please refer to the supplementary material.

We compare RISA-Net with other alternative approaches, including Spherical Harmonics descriptor (SHD) [7], LightField descriptor (LFD) [6], MVCNN [14], RotationNet [41], spherical CNNs [20], SeqViews2SeqLabels (SVSL) [17] and MeshCNN [33]. For both MVCNN and SeqViews2SeqLabels, we render 12 views of the shape, as reported in their best results. For RotationNet, we use the same camera setting as *case(ii)* in their paper, which places cameras on vertices of a dodecahedron encompassing the object. For spherical CNNs, we use in-batch triplet loss for retrieval. For MeshCNN, we use the output of the classification network as the shape descriptor, and rank the shape descriptors by their Euclidean distance to the

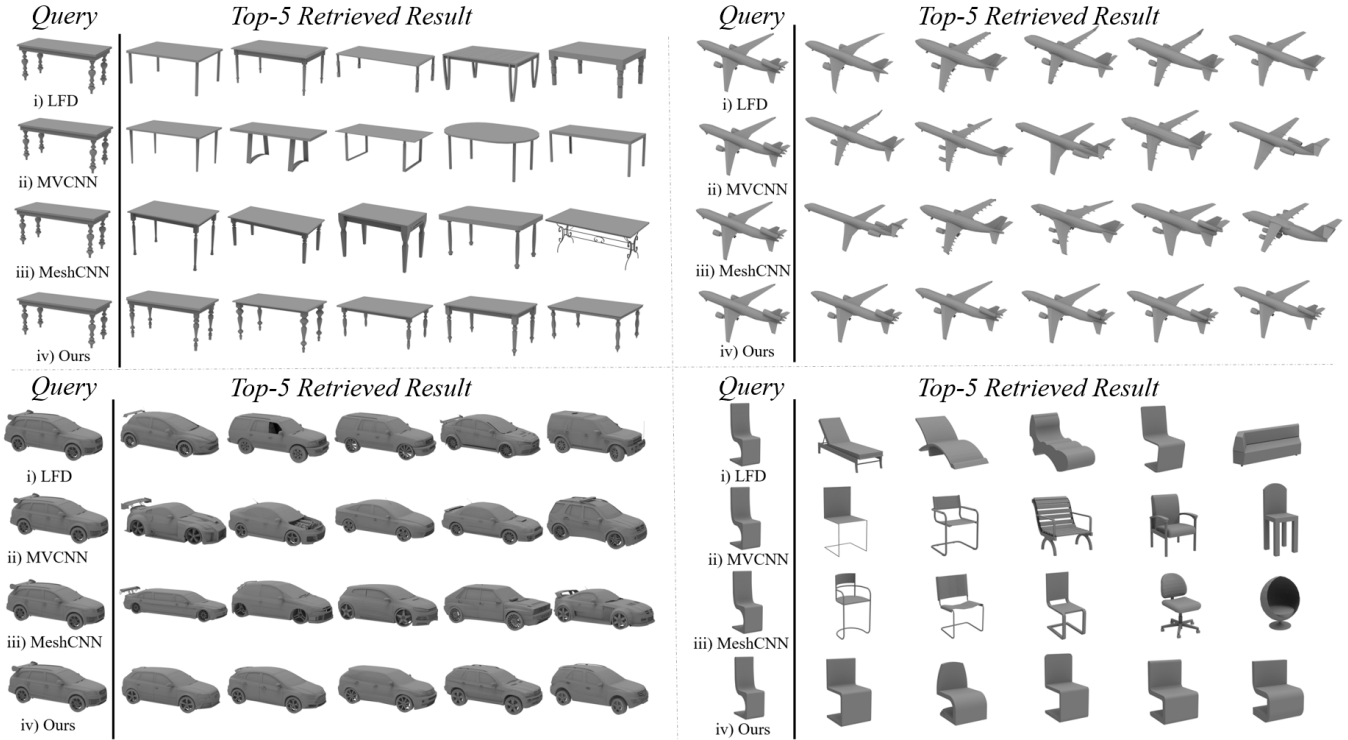


Fig. 6: Visual comparison of retrieval results among LFD, MVCNN, MeshCNN and our method. Our method outperforms the other methods on geometric local feature encoding and fine-grained object retrieval.

query to measure shape similarity. All the above methods are evaluated on our perturbed dataset. Fig. 5 visualizes the comparative results on the test set of RISA-Net and other methods with the PR (Precision-Recall) Curves for the six object categories. The performance of the learned descriptors by other methods varies among categories. The performances of SHD and LFD are more stable than learning-based methods. The PR curves show that RISA-Net clearly outperforms other methods on all categories in terms of both precision and recall.

Table 2 shows the quantitative comparison between RISA-Net and other methods on six object categories. We conduct quantitative experiment on fine-grained shape retrieval. Both query shapes and repository come from the test set to ensure fairness. The results are evaluated using various statistical metrics: Nearest Neighbor (NN), First Tier (FT), Second Tier (ST), Normalized Discounted Cumulative Gain (NDCG) and mean Averaged Precision (mAP). Considering the imbalance of model numbers of the sub-classes, each measure is calculated through both micro and macro average. The macro averaging computes the metric independently for each sub-class and then takes their average as the final overall metric, whereas the micro averaging is a weighted average with the weight for each sub-category proportional to the number of objects in it. Table 2 demonstrates the performances of RISA-Net and other methods on the six categories of objects. Noticeably, mesh-based deep models, MeshCNN [33] and our method outperform other methods on almost all of the metrics. Apart from these two methods, MVCNN [14] and LFD [6] are better than other methods on all of the metrics. Overall, RISA-Net achieves the best performance among all alternative methods under

all the above metrics.

Fig. 6 provides examples of top-5 retrieved results by using LFD, MVCNN, MeshCNN and RISA-Net respectively. In the top-left example, the query shape is a traditional rectangular dining table with turned legs. The retrieved models by LFD are with the similar height, surface and leg numbers, which match the coarse-level features of the query shape. MVCNN returned models are with similar height but failed to recognize the rectangular top and turned legs. MeshCNN found rectangular tables with decorated legs, but the shapes of their legs do not match the query, and some tables are obviously taller than the query table. Only RISA-Net successfully recognized the turned table legs, showing its superiority on encoding fine-grained geometric features. In the top-right example, though all three methods retrieve globally similar planes, only RISA-Net identified the discriminative feature on the tail of the query plane and retrieved shapes of the same sub-class, showing its capability of recognizing discriminative parts. In the bottom-left example, the query shape is a hatch-back car, however, most of LFD’s retrieved results are minivans, most of MVCNN’s retrieved results are sedans, and only some of MeshCNN’s retrieved cars are visually similar to the query shapes. Our method not only returned results that are all hatch-backs rather than cars from other sub-classes, but also returned hatch-backs with wheels similar to the query shape. In the bottom-right example, robustness to rigid transformation and the balanced structure/geometric information enabled our method to retrieve chairs of the same sub-class, but other methods mostly failed.

In Fig. 7, we use a tier image [61] to visualize the global retrieval results of our method. In a tier image, each row

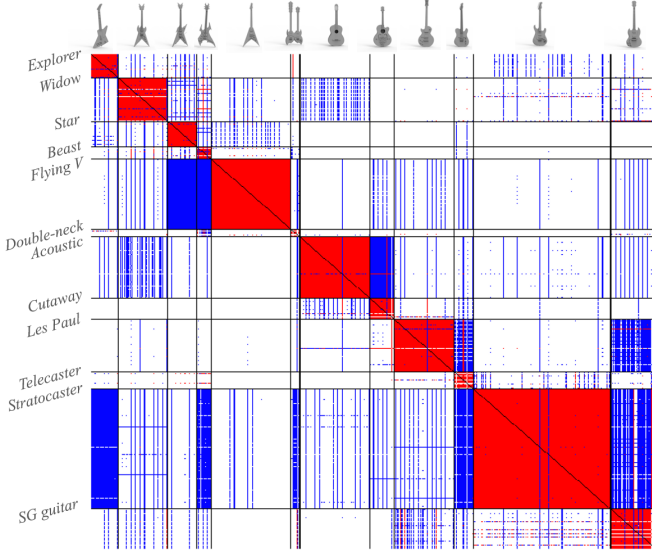


Fig. 7: Illustration of the tier image of our result for the dataset of guitar.

represents a query with model j . Pixel (i, j) is filled by black, red, and blue if model i is the nearest neighbor, first tier match, and the second tier match of j respectively. Along each axis, models are grouped by sub-class, and lines are added to separate each sub-class. In each sub-class, red pixels are clustered in blocks along the diagonal, showing that models of the same sub-class are each other’s first tier matching results. Moreover, second tier matches of each sub-class tend to congregate together in the same block, implying that RISA-Net learns the similarity between sub-classes. For example, most second tier matches of *Les Paul* are under the sub-class of *Telecaster* and *SG guitar*. It can be observed that the three sub-classes of guitar share many local features as shown by the illustrated randomly selected instances. Both *Telecaster* and *SG guitar* are electric guitars that have a thin solid body as *Les Paul*. Also, these guitars have similar round shapes in their lower-half bodies and missing cuts on their upper half bodies.

4.4 Weighted Features of Parts by Part-Geo Attention

Our model utilizes the *Part-Geo* attention mechanism to balance the contributions of different parts when discerning a shape among sub-classes. Fig. 8 visualizes the learned attention information that demonstrates the importance of each part when learning the final latent descriptor, where we highlight the valid parts using the learned attention weights. Note that the weights of missing parts are set to 0. Aside from those missing parts, the discriminative parts of the shapes are successfully assigned with relatively high weights, meaning that they contribute more than the other parts to the latent feature learning. More specifically, in Fig. 8(a), the highest weight of each plane appears on the most discriminative part: engine, wing, tail or body. In Fig. 8(b), the weights of existing parts also conform to their discriminativeness. The highest weights are assigned to leg, arm, back and seat respectively.

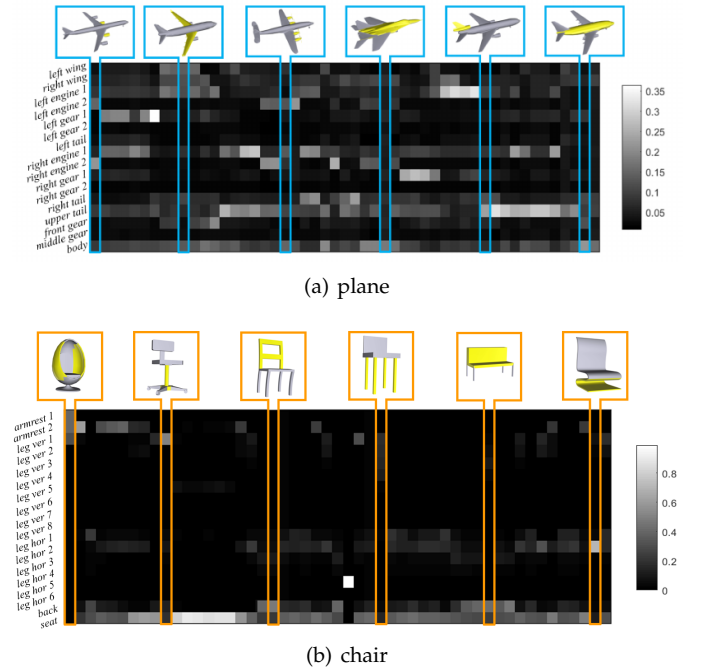


Fig. 8: Part geometry attention visualization on the plane and chair datasets.

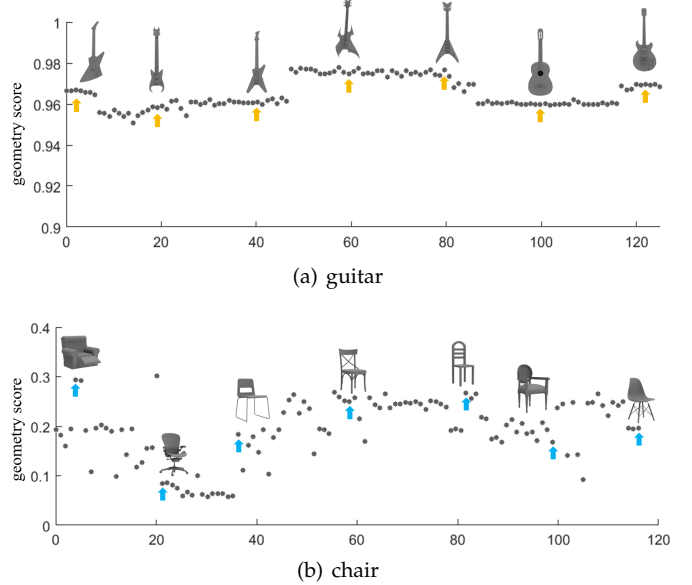


Fig. 9: Visualization of geometry-structure attention information on guitar and chair datasets.

4.5 Weighted Features by Geo-Struct Attention

The *Geo-Struct* attention mechanism balances the geometry and structure information in our shape representation. Fig. 8 visualizes the learned geometry score w^g in guitar and chair datasets. The structure score is calculated by: $w^s = 1 - w^g$. In each dataset, we randomly selected some model in the test set. Models are grouped by sub-classes along x -axis, and their geometry scores are shown by their y -coordinates. Each point represents an object instance, and we draw the 3D shapes of several representative instances

for better visualization. Note that shapes of the same subclass that share similar structure/geometry features tend to have similar structure/geometry scores. Also, the average geometry score of the class of guitar is higher than chair, indicating that distinguishing guitars relies more on geometric information than chairs.

4.6 Generalizability

Performance on other public datasets. To validate the ability of RISA-Net to generalize to other public datasets, we manually segmented the test dataset of the guitar category of ModelNet40, which contains 100 guitar models. All segmented parts are registered from a unit cube with 3075 vertex in a coarse-to-fine manner [54]. Then, using the network trained on our dataset, we feed the manually segmented mesh directly to the trained model without any fine-tuning operation. Some results are illustrated in Fig. 10, which demonstrate that RISA-Net is capable of learning effective features that generalize well to new datasets.

Retrieval with fully-automatic part segmentation. In this experiment, we investigate whether our approach is sufficiently practical to be combined with existing shape segmentation methods to retrieve a shape without pre-segmentation. Instead of manually segmenting the shapes into parts, we use the following way to automatically obtain the segmentation results. We randomly and uniformly sampled 2048 points from each watertight mesh, and then feed the points to PointNet++ [51] for segmentation. The segmentation accuracy (the ratio of the correctly segmented) on guitar and plane datasets are 92.46% and 89.29% respectively. With the semantically labeled points from PointNet, we align watertight mesh models to the points and assign each triangular mesh with the label of the closest point. Then we use the segmented meshes to train and test our model. Fig. 11 shows the PR curves of RISA-Net’s performance on

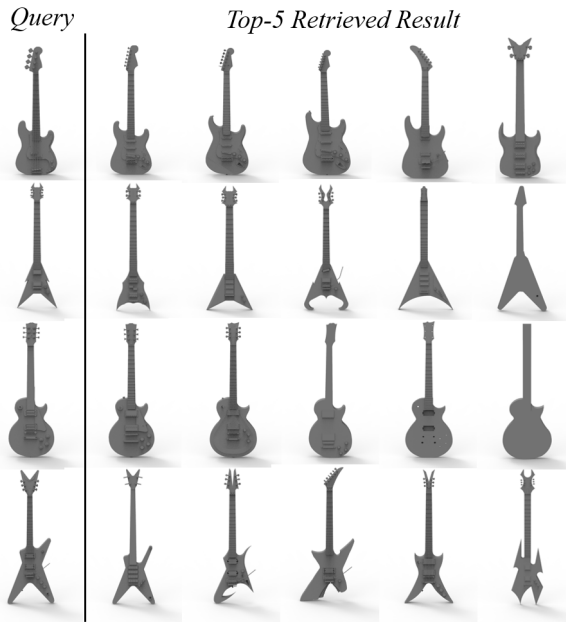


Fig. 10: Examples of top-5 retrieval results on the test set of ModelNet guitar dataset.

the datasets of guitar and plane using models without pre-segmentation (*Ours(v2)*), compared with the pre-segmented models (*Ours(v1)*). We also display the PR curves of other methods for comparison. Note that our approach is able to tolerate minor part segmentation errors, indicating its capability to be used in real world shape retrieval applications.

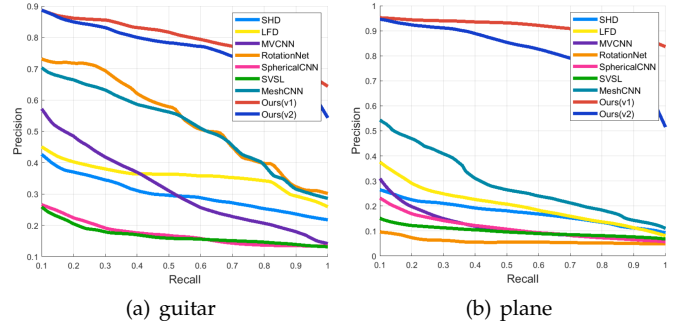


Fig. 11: PR curves on guitar and plane datasets using models without pre-segmentation

4.7 Ablation Study

We now provide the results of a detailed ablation study that shows the contribution of each component to the overall performance, including base geometric feature selection, the feature extractor selection and the hierarchical structure.

Geometric feature extraction. In this subsection, we show the effectiveness of the adopted scale-sensitive features and a reconstructive network to describe part geometry. We design a comparison group that replaces our base geometric feature with the 5 dimensional shape feature proposed by Hanocka et al. [33] as a scale-insensitive feature, which is denoted as “Ours(scale sensitive)”. We design another comparison group by replacing *PartVAEs* with the classification network in [33], which is denoted as “Ours(CNN)”. The PR curves of fine-grained retrieval results on the table category with these three configurations are demonstrated in Fig. 12. It shows that the scale-sensitive base feature is more suitable for our framework, and the reconstructive network is better for detailed geometric information learning.

We also provide two examples for visual comparison. Fig. 13(a) is a comparison of different choices of base features. Using the scale-invariant feature as in MeshCNN [33], although the semantic parts of retrieved shapes all look similar to the parts of the query shape, the size relationship is not maintained among parts, leading to dissimilar overall shapes. In Fig. 13(b), a failure case of using CNN instead of our *PartVAE* structure is provided. Using the classification network for feature extraction sometimes fails to capture geometric features from thin geometry. In contrast, with the reconstructive network of our *PartVAE*, the detailed geometric features are well-learned in the latent space of our VAE modules as shown in the experiment, showing the effectiveness of our *PartVAEs*.

Variational AutoEncoder vs. AutoEncoder. In our observations, the part-wise differences are the key factors to distinguish between sub-classes, because the shapes of the

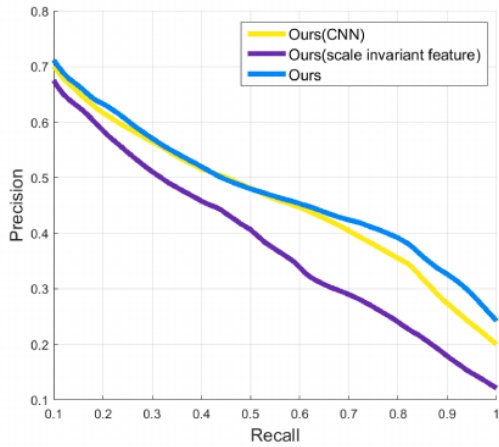


Fig. 12: The PR curves comparing different base features and geometric feature extractors on the table dataset.



(a) Comparison between scale-invariant and scale-sensitive feature as base geometric feature



(b) Comparison between classification network and reconstructive network as base geometric feature extractor.

Fig. 13: Top-5 retrieved results among different base features and geometric feature extractors.

same class share similar global structural features. That could be better modeled by VAE, because it is able to learn shape representations with such disentangled factors. We compare the performance by replacing the Variational AutoEncoder by a normal AutoEncoder in our model for validation. The performance of fine-grained retrieval of latent features learned by the VAE-based and AE-based models are given in Table 3. The VAE-based approach achieves a significantly better result than AE-based approach.

TABLE 3: The comparison between VAE and AE structure, $latent_1 = 64$, $latent_2 = 64$.

micro					
Methods	NN	FT	ST	NDCG	mAP
AE	0.6972	0.5433	0.6191	0.7457	0.5777
VAE	0.7378	0.5670	0.6892	0.7878	0.6125
macro					
Methods	NN	FT	ST	NDCG	mAP
AE	0.5248	0.4420	0.5119	0.6329	0.4801
VAE	0.6003	0.4642	0.5631	0.7065	0.5142

Structure information. Finally, we compare the performance of RISA-Net with and without structural information in shape description. To remove the structural information, we just encode geometric information through the set of *PartVAEs* and *Part-Geo* attention mechanism, and feed their concatenation to the *GlobalVAE* to form the final shape descriptor. As shown in Table 4, the shape descriptor that contains global structure information has a better performance than the shape descriptor with only geometric information.

TABLE 4: The comparison between RISA-Net with and without structure information, $lr = 1 \times 10^{-5}$, $latent_1 = 64$, $latent_2 = 64$.

micro					
Methods	NN	FT	ST	NDCG	mAP
PartVAE Set	0.7038	0.5011	0.5880	0.7598	0.5754
RISA-Net	0.7378	0.5670	0.6892	0.7878	0.6125
macro					
Methods	NN	FT	ST	NDCG	mAP
PartVAE Set	0.5841	0.4092	0.4976	0.6767	0.4752
RISA-Net	0.6003	0.4642	0.5631	0.7065	0.5142

4.8 Limitations and Future work

RISA-Net encodes structural information based on the spatial relationships between semantic parts, which leads to a need for correspondences between the segmented parts of the query shape and the dataset. Therefore, if the query object has totally different topology with the data in the repository, RISA-Net may fail to interpret the structural information effectively. Further research can focus on how to automatically learn the structural information and combine it with geometric information.

5 CONCLUSION

In this paper, we introduce RISA-Net, a novel framework to extract shape descriptors for fine-grained 3D object retrieval. RISA-Net is able to extract 3D shape descriptors with geometric details and global structural information, which are invariant to rigid transformation. Trained with the attention mechanisms and the dedicatedly designed losses, RISA-Net can locate and emphasize discriminative parts, and make a balance between structure and geometric information when representing a 3D shape. Thanks to the above designs, the Through fruitful experiments on fine-grained 3D shape retrieval, we demonstrated that RISA-Net outperforms the state of the art on fine-grained 3D object retrieval task. For future work, fine-grained sketch-based and image-based object retrieval would be a natural extension to our work. Also, with our method retrieving fine-grained similar shapes, how to utilize the retrieved shapes for modeling of new shapes is worth also exploring.

REFERENCES

- [1] N. Duncan, L.-F. Yu, and S.-K. Yeung, "Interchangeable components for hands-on assembly based modelling," *ACM Transactions on Graphics (TOG)*, vol. 35, no. 6, pp. 1–14, 2016.
- [2] W. Shen, D. H. Norrie, and J.-P. Barthès, *Multi-agent systems for concurrent intelligent design and manufacturing*. CRC press, 2003.

- [3] X. Xie, K. Xu, N. J. Mitra, D. Cohen-Or, W. Gong, Q. Su, and B. Chen, "Sketch-to-design: Context-based part assembly," in *Computer Graphics Forum*, vol. 32, no. 8. Wiley Online Library, 2013, pp. 233–245.
- [4] M. A. Uy, J. Huang, M. Sung, T. Birdal, and L. Guibas, "Deformation-aware 3D model embedding and retrieval," *arXiv preprint arXiv:2004.01228*, 2020.
- [5] K. Xu, K. Chen, H. Fu, W.-L. Sun, and S.-M. Hu, "Sketch2Scene: sketch-based co-retrieval and co-placement of 3D models," *ACM Transactions on Graphics (TOG)*, vol. 32, no. 4, pp. 1–15, 2013.
- [6] D.-Y. Chen, X.-P. Tian, Y.-T. Shen, and M. Ouhyoung, "On visual similarity based 3D model retrieval," in *Computer graphics forum*, vol. 22, no. 3. Wiley Online Library, 2003, pp. 223–232.
- [7] M. Kazhdan, T. Funkhouser, and S. Rusinkiewicz, "Rotation invariant spherical harmonic representation of 3D shape descriptors," in *Symposium on geometry processing*, vol. 6, 2003, pp. 156–164.
- [8] R. Osada, T. Funkhouser, B. Chazelle, and D. Dobkin, "Shape distributions," *ACM Transactions on Graphics (TOG)*, vol. 21, no. 4, pp. 807–832, 2002.
- [9] J. Sun, M. Ovsjanikov, and L. Guibas, "A concise and provably informative multi-scale signature based on heat diffusion," in *Computer graphics forum*, vol. 28, no. 5. Wiley Online Library, 2009, pp. 1383–1392.
- [10] I. Pratikakis, M. Spagnuolo, T. Theoharis, and R. Veltkamp, "Learning the compositional structure of man-made objects for 3D shape retrieval," in *Eurographics Workshop on 3D Object Retrieval (2010)*, 2010.
- [11] A. M. Bronstein, M. M. Bronstein, L. J. Guibas, and M. Ovsjanikov, "Shape google: Geometric words and expressions for invariant shape retrieval," *ACM Transactions on Graphics (TOG)*, vol. 30, no. 1, pp. 1–20, 2011.
- [12] C. Redondo-Cabrera, R. J. Lopez-Sastre, J. Acevedo-Rodriguez, and S. Maldonado-Bascon, "Surfing the point clouds: Selective 3D spatial pyramids for category-level object recognition," in *2012 IEEE Conference on Computer Vision and Pattern Recognition*. IEEE, 2012, pp. 3458–3465.
- [13] R. Ohbuchi and T. Furuya, "Distance metric learning and feature combination for shape-based 3D model retrieval," in *Proceedings of the ACM workshop on 3D object retrieval*, 2010, pp. 63–68.
- [14] H. Su, S. Maji, E. Kalogerakis, and E. Learned-Miller, "Multi-view convolutional neural networks for 3D shape recognition," in *Proceedings of the IEEE international conference on computer vision*, 2015, pp. 945–953.
- [15] S. Bai, X. Bai, Z. Zhou, Z. Zhang, and L. Jan Latecki, "Gift: A real-time and scalable 3D shape search engine," in *Proceedings of the IEEE conference on computer vision and pattern recognition*, 2016, pp. 5023–5032.
- [16] A. Kanezaki, Y. Matsushita, and Y. Nishida, "Rotationnet: Joint object categorization and pose estimation using multiviews from unsupervised viewpoints," in *Proceedings of the IEEE Conference on Computer Vision and Pattern Recognition*, 2018, pp. 5010–5019.
- [17] Z. Han, M. Shang, Z. Liu, C.-M. Vong, Y.-S. Liu, M. Zwicker, J. Han, and C. P. Chen, "Seqviews2seqlabels: Learning 3D global features via aggregating sequential views by RNN with attention," *IEEE Transactions on Image Processing*, vol. 28, no. 2, pp. 658–672, 2018.
- [18] Z. Han, H. Lu, Z. Liu, C.-M. Vong, Y.-S. Liu, M. Zwicker, J. Han, and C. P. Chen, "3d2seqviews: Aggregating sequential views for 3D global feature learning by CNN with hierarchical attention aggregation," *IEEE Transactions on Image Processing*, vol. 28, no. 8, pp. 3986–3999, 2019.
- [19] B. Shi, S. Bai, Z. Zhou, and X. Bai, "Deeppano: Deep panoramic representation for 3-d shape recognition," *IEEE Signal Processing Letters*, vol. 22, no. 12, pp. 2339–2343, 2015.
- [20] C. Esteves, C. Allen-Blanchette, A. Makadia, and K. Daniilidis, "Learning so (3) equivariant representations with spherical cnns," in *Proceedings of the European Conference on Computer Vision (ECCV)*, 2018, pp. 52–68.
- [21] T. Furuya and R. Ohbuchi, "Deep aggregation of local 3D geometric features for 3D model retrieval," in *BMVC*, vol. 7, 2016, p. 8.
- [22] Y. Zhou and O. Tuzel, "VoxelNet: End-to-end learning for point cloud based 3D object detection," in *Proceedings of the IEEE Conference on Computer Vision and Pattern Recognition*, 2018, pp. 4490–4499.
- [23] B. Li, A. Godil, M. Aono, X. Bai, T. Furuya, L. Li, R. J. López-Sastre, H. Johan, R. Ohbuchi, C. Redondo-Cabrera *et al.*, "SHREC'12 track: Generic 3D shape retrieval," in *3DOR*, vol. 6, 2012.
- [24] M. Savva, F. Yu, H. Su, M. Aono, B. Chen, D. Cohen-Or, W. Deng, H. Su, S. Bai, X. Bai *et al.*, "SHREC16 track: largescale 3D shape retrieval from ShapeNet core55," in *Proceedings of the eurographics workshop on 3D object retrieval*, vol. 10, 2016.
- [25] J. Masci, D. Boscaini, M. Bronstein, and P. Vandergheynst, "Geodesic convolutional neural networks on riemannian manifolds," in *Proceedings of the IEEE international conference on computer vision workshops*, 2015, pp. 37–45.
- [26] A. Sinha, J. Bai, and K. Ramani, "Deep learning 3D shape surfaces using geometry images," in *European Conference on Computer Vision*. Springer, 2016, pp. 223–240.
- [27] D. Boscaini, J. Masci, E. Rodolà, and M. Bronstein, "Learning shape correspondence with anisotropic convolutional neural networks," in *Advances in neural information processing systems*, 2016, pp. 3189–3197.
- [28] F. Monti, D. Boscaini, J. Masci, E. Rodola, J. Svoboda, and M. M. Bronstein, "Geometric deep learning on graphs and manifolds using mixture model CNNs," in *Proceedings of the IEEE Conference on Computer Vision and Pattern Recognition*, 2017, pp. 5115–5124.
- [29] D. Boscaini, J. Masci, S. Melzi, M. M. Bronstein, U. Castellani, and P. Vandergheynst, "Learning class-specific descriptors for deformable shapes using localized spectral convolutional networks," in *Computer Graphics Forum*, vol. 34, no. 5. Wiley Online Library, 2015, pp. 13–23.
- [30] J. Xie, M. Wang, and Y. Fang, "Learned binary spectral shape descriptor for 3D shape correspondence," in *Proceedings of the IEEE Conference on Computer Vision and Pattern Recognition*, 2016, pp. 3309–3317.
- [31] Z. Han, Z. Liu, J. Han, C.-M. Vong, S. Bu, and X. Li, "Unsupervised 3D local feature learning by circle convolutional restricted Boltzmann machine," *IEEE Transactions on Image Processing*, vol. 25, no. 11, pp. 5331–5344, 2016.
- [32] Z. Han, Z. Liu, J. Han, C.-M. Vong, S. Bu, and C. L. P. Chen, "Mesh convolutional restricted boltzmann machines for unsupervised learning of features with structure preservation on 3-D meshes," *IEEE transactions on neural networks and learning systems*, vol. 28, no. 10, pp. 2268–2281, 2016.
- [33] R. Hanocka, A. Hertz, N. Fish, R. Giryes, S. Fleishman, and D. Cohen-Or, "MeshCNN: a network with an edge," *ACM Transactions on Graphics (TOG)*, vol. 38, no. 4, pp. 1–12, 2019.
- [34] J. Schult, F. Engelmann, T. Kontogianni, and B. Leibe, "DualConvMesh-Net: Joint geodesic and euclidean convolutions on 3d meshes," *arXiv preprint arXiv:2004.01002*, 2020.
- [35] J. Xie, G. Dai, F. Zhu, E. K. Wong, and Y. Fang, "DeepShape: Deep-learned shape descriptor for 3d shape retrieval," *IEEE transactions on pattern analysis and machine intelligence*, vol. 39, no. 7, pp. 1335–1345, 2016.
- [36] O. Litany, A. Bronstein, M. Bronstein, and A. Makadia, "Deformable shape completion with graph convolutional autoencoders," in *Proceedings of the IEEE conference on computer vision and pattern recognition*, 2018, pp. 1886–1895.
- [37] Z. Han, Z. Liu, C.-M. Vong, Y.-S. Liu, S. Bu, J. Han, and C. P. Chen, "Deep spatiality: Unsupervised learning of spatially-enhanced global and local 3D features by deep neural network with coupled softmax," *IEEE Transactions on Image Processing*, vol. 27, no. 6, pp. 3049–3063, 2018.
- [38] L. Gao, J. Yang, T. Wu, Y.-J. Yuan, H. Fu, Y.-K. Lai, and H. Zhang, "SDM-NET: Deep generative network for structured deformable mesh," *ACM Transactions on Graphics (TOG)*, vol. 38, no. 6, pp. 1–15, 2019.
- [39] R. Wu, Y. Zhuang, K. Xu, H. Zhang, and B. Chen, "PQ-NET: A generative part seq2seq network for 3D shapes," *arXiv preprint arXiv:1911.10949*, 2019.
- [40] C. R. Qi, H. Su, M. Nießner, A. Dai, M. Yan, and L. J. Guibas, "Volumetric and multi-view CNNs for object classification on 3D data," in *Proceedings of the IEEE conference on computer vision and pattern recognition*, 2016, pp. 5648–5656.
- [41] N. Thomas, T. Smidt, S. Kearnes, L. Yang, L. Li, K. Kohlhoff, and P. Riley, "Tensor field networks: Rotation-and translation-equivariant neural networks for 3D point clouds," *arXiv preprint arXiv:1802.08219*, 2018.
- [42] D. E. Worrall, S. J. Garbin, D. Turmukhambetov, and G. J. Brostow, "Harmonic networks: Deep translation and rotation equivariance," in *Proceedings of the IEEE Conference on Computer Vision and Pattern Recognition*, 2017, pp. 5028–5037.
- [43] X. Zhang, S. Qin, Y. Xu, and H. Xu, "Quaternion product

units for deep learning on 3D rotation groups,” *arXiv preprint arXiv:1912.07791*, 2019.

- [44] J. F. Henriques and A. Vedaldi, “Warped convolutions: Efficient invariance to spatial transformations,” in *Proceedings of the 34th International Conference on Machine Learning-Volume 70*. JMLR.org, 2017, pp. 1461–1469.
- [45] T. Cohen and M. Welling, “Group equivariant convolutional networks,” in *International conference on machine learning*, 2016, pp. 2990–2999.
- [46] D. Worrall and G. Brostow, “CubeNet: Equivariance to 3D rotation and translation,” in *Proceedings of the European Conference on Computer Vision (ECCV)*, 2018, pp. 567–584.
- [47] T. S. Cohen, M. Weiler, B. Kicanaoglu, and M. Welling, “Gauge equivariant convolutional networks and the icosahedral CNN,” *arXiv preprint arXiv:1902.04615*, 2019.
- [48] C. Esteves, Y. Xu, C. Allen-Blanchette, and K. Daniilidis, “Equivariant multi-view networks,” in *Proceedings of the IEEE International Conference on Computer Vision*, 2019, pp. 1568–1577.
- [49] T. S. Cohen, M. Geiger, J. Köhler, and M. Welling, “Spherical CNNs,” *arXiv preprint arXiv:1801.10130*, 2018.
- [50] C. R. Qi, H. Su, K. Mo, and L. J. Guibas, “PointNet: Deep learning on point sets for 3D classification and segmentation,” in *Proceedings of the IEEE conference on computer vision and pattern recognition*, 2017, pp. 652–660.
- [51] C. R. Qi, L. Yi, H. Su, and L. J. Guibas, “PointNet++: Deep hierarchical feature learning on point sets in a metric space,” in *Advances in neural information processing systems*, 2017, pp. 5099–5108.
- [52] H. Deng, T. Birdal, and S. Ilic, “PPFNet: Global context aware local features for robust 3D point matching,” in *Proceedings of the IEEE Conference on Computer Vision and Pattern Recognition*, 2018, pp. 195–205.
- [53] S. Fröhlich and M. Botsch, “Example-driven deformations based on discrete shells,” in *Computer graphics forum*, vol. 30, no. 8. Wiley Online Library, 2011, pp. 2246–2257.
- [54] M. Zollhöfer, M. Nießner, S. Izadi, C. Rehmann, C. Zach, M. Fisher, C. Wu, A. Fitzgibbon, C. Loop, C. Theobalt *et al.*, “Real-time non-rigid reconstruction using an RGB-D camera,” *ACM Transactions on Graphics (ToG)*, vol. 33, no. 4, pp. 1–12, 2014.
- [55] A. Vaswani, N. Shazeer, N. Parmar, J. Uszkoreit, L. Jones, A. N. Gomez, Ł. Kaiser, and I. Polosukhin, “Attention is all you need,” in *Advances in neural information processing systems*, 2017, pp. 5998–6008.
- [56] F. Schroff, D. Kalenichenko, and J. Philbin, “FaceNet: A unified embedding for face recognition and clustering,” in *Proceedings of the IEEE conference on computer vision and pattern recognition*, 2015, pp. 815–823.
- [57] Z. Wu, S. Song, A. Khosla, F. Yu, L. Zhang, X. Tang, and J. Xiao, “3D ShapeNets: A deep representation for volumetric shapes,” in *Proceedings of the IEEE conference on computer vision and pattern recognition*, 2015, pp. 1912–1920.
- [58] A. X. Chang, T. Funkhouser, L. Guibas, P. Hanrahan, Q. Huang, Z. Li, S. Savarese, M. Savva, S. Song, H. Su *et al.*, “ShapeNet: An information-rich 3D model repository,” *arXiv preprint arXiv:1512.03012*, 2015.
- [59] P. J. Phillips, P. J. Flynn, T. Scruggs, K. W. Bowyer, J. Chang, K. Hoffman, J. Marques, J. Min, and W. Worek, “Overview of the face recognition grand challenge,” in *2005 IEEE computer society conference on computer vision and pattern recognition (CVPR’05)*, vol. 1. IEEE, 2005, pp. 947–954.
- [60] D. P. Kingma and J. Ba, “Adam: A method for stochastic optimization,” *arXiv preprint arXiv:1412.6980*, 2014.
- [61] P. Shilane, P. Min, M. Kazhdan, and T. Funkhouser, “The Princeton shape benchmark,” in *Proceedings Shape Modeling Applications*, 2004. IEEE, 2004, pp. 167–178.



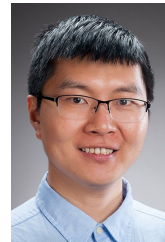
Rao Fu is now a bachelor candidate in the University of Chinese Academy of Sciences, majoring in computer science. She has been a visiting researcher in University of California, San Diego. Her research interests include computer graphics, geometric processing and 3D computer vision.



Jie Yang received a bachelor’s degree in mathematics from Sichuan University in 2016. He is currently a PhD candidate in the Institute of Computing Technology, Chinese Academy of Sciences. His research interests include computer graphics and geometric processing.



Jiawei Sun is now majoring in computer science. She is currently an undergraduate in Beijing Jiaotong University. Her research interests include computer graphics and geometric processing.



Fang-Lue Zhang is currently a lecturer with Victoria University of Wellington, New Zealand. He received the Bachelors degree from Zhejiang University, Hangzhou, China, in 2009, and the Doctoral degree from Tsinghua University, Beijing, China, in 2015. His research interests include image and video editing, computer vision, and computer graphics. He is a member of IEEE and ACM. He received Victoria Early Career Research Excellence Award in 2019.



Yu-Kun Lai received his bachelor’s degree and PhD degree in computer science from Tsinghua University in 2003 and 2008, respectively. He is currently a Professor in the School of Computer Science & Informatics, Cardiff University. His research interests include computer graphics, geometry processing, image processing and computer vision. He is on the editorial boards of *Computer Graphics Forum* and *The Visual Computer*.



Lin Gao received the bachelor’s degree in mathematics from Sichuan University and the PhD degree in computer science from Tsinghua University. He is currently an Associate Professor at the Institute of Computing Technology, Chinese Academy of Sciences. He has been awarded the Newton Advanced Fellowship from the Royal Society and the AG young researcher award. His research interests include computer graphics and geometric processing.

SUPPLEMENTARY MATERIAL

1 FINE-GRAINED 3D OBJECT RETRIEVAL DATASET

Our 3D object dataset for validating fine-grained retrieval is built based on the dataset of SDM-NET [38]. It contains 8906 3D models of six object categories, which are cars, planes, chairs, tables, guitars and knives. Each category is further manually classified into sub-classes based on the functionality and style.

1.1 Annotation Method

We adopt three steps to categorize each object category into sub-classes. Firstly, we manually divide the shapes of the same category into sub-classes according to their intra-class features, such as functionality, designation style and product model number. We leverage our classification with ShapeNet’s taxonomy, and assign each sub-class with different semantic labels. A few sub-classes are assigned a label of product number by one of its representing objects. Secondly, we clean-up the dataset by discarding unrealistic models and special models that do not have similar features with any named sub-classes. Finally, we inspect the labels to make sure the preciseness of shapes under each sub-class.

1.2 Dataset Examples

Figure 14 - Figure 19 illustrate several examples of some sub-classes of each category. Note that objects of each sub-class share similar high-level structural features, but have distinguishable part-wise features. For example, in Figure 14, the four sub-classes of cars have similar overall structures, but cars of the sub-class “F1 race car” are single-seated, open cockpit racing cars, and cars that are labeled by “crew cab pickup” are pickups with a single row of seats.

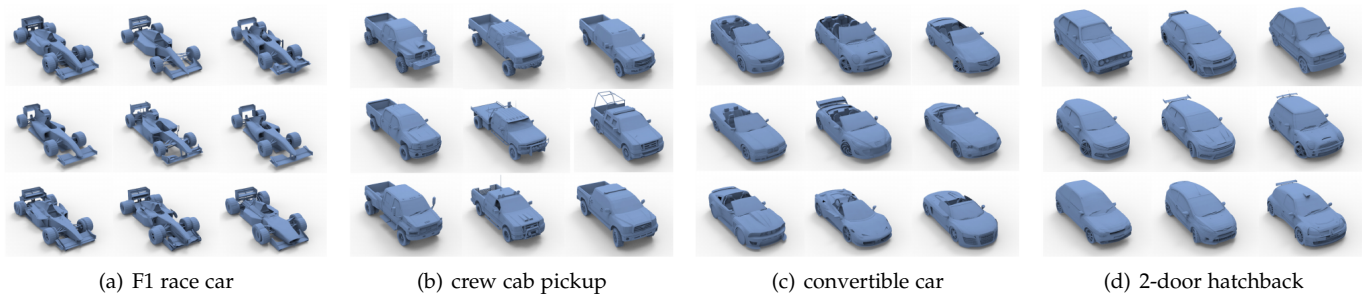


Fig. 14: Examples of four sub-classes of cars.

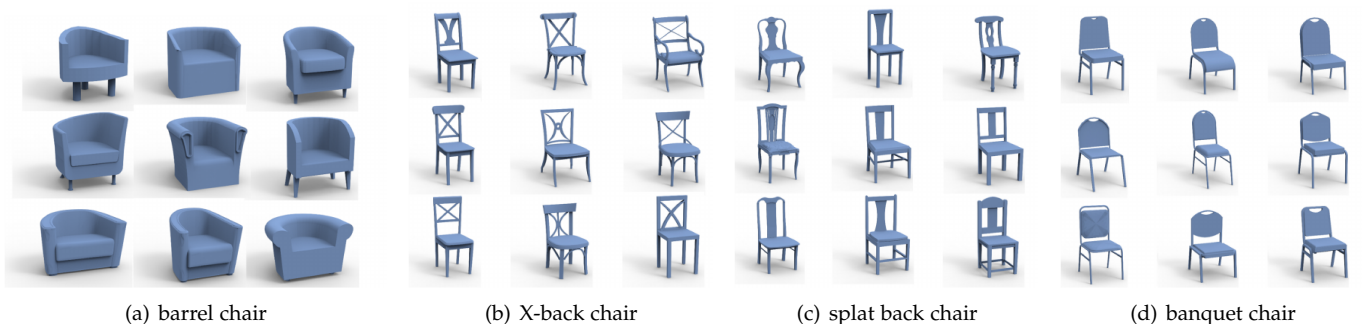


Fig. 15: Examples of four sub-classes of chairs.

1.3 Sub-class Distribution

Table 5-Table 6 provide the number of shapes under each sub-class on six object categories. Fig. 20 illustrate the sub-class distribution, ranked by the number of models from high to low.

TABLE 5: Statistics of sub-classes of 3 categories.

Car		Plane				Chair			
Sub-Class	Num	Sub-Class	Num	Sub-Class	Num	Sub-Class	Num	Sub-Class	Num
sedan	219	A320	181	BAe 146	16	tucker	314	elbow chair	17
sports car	140	B747	158	B737-200	15	straight chair	251	x-back	16
convertible cars	106	CRJ	153	A300-600	15	conference chair	201	outdoor lounge	14
extended cab pickup	100	B737-800	142	B767-300w	13	slat chair	146	sofa	13
crew cab pickup	93	B777-300	89	E170	12	lounge chair	116	bench	13
supercar	85	DC10	84	Lockheed F117	11	prouve chair	113	norman chair	13
2-door hatchback	83	A340-600	79	E195	10	sqaure back chair	102	barrel chair	11
coupe	80	A330-300	78	Concorde	10	parson chair	98	arne jacobsen egg chair	11
vintage muscle car	72	B787-800	67	MIG15	10	cantilever side chair	90	cantilever lounge chair	11
minivan	55	B727	67	B737-600	9	sled base chair	68	bentwood chairs	11
regular cab pickup	43	Lockheed Martin X-35	60	Cessna C208	9	ladder back	65	banquet chair	10
4-door hatchback	35	middle wing propeller	54	Super Transport	4	high stool chair	62	park bench	10
coach bus	29	A380	54			club chair	56	windsor chair	9
f1 race car	29	B767-300	48			vintage french	55	eiffel aimchair	8
convertible vintage	27	B777-200	47			revolving chair	52	chiavari chairs	7
luxury car	25	high wing propeller	44			splat back chair	48	industrial café	6
cargo van	19	B757-200	42			adirondack	35	easter egg chair	5
off-roader	19	P51 Musang	36			navy chair	35	outdoor iron chair	5
muv	17	B737-832	34			folding chair	32		
cargo truck	16	B707	28			task chair	31		
suv	16	L-1011 Tristar	21			qing chair	29		
truck tractor	15	B737-2VG	19			panton chair	27		
all-terrain vehicle	13	B757-200w	19			eiffel chair	22		
stretched limo	12	B737-300	18			drafting chair	20		
stretched suv	7	E190	17			slipper chair	19		
semi-trailer truck	6	Rafale	17			barcelona chair	18		
school bus	4	MIRAGE 2000	17			rocking chair	17		
Total	1365				1807				2312

TABLE 6: Statistics of sub-classes of 3 categories.

Knife		Guitar		Table			
Sub-Class	Num	Sub-Class	Num	Sub-Class	Num	Sub-Class	Num
sword	54	Stratocaster	153	modern rectangular dining table	259	frame rectangular dinner table	49
combat knife	37	Gibson Flying V	89	classic rectangular end table	192	pool table	40
machete	21	acoustic guitar	78	pedestal round end table	173	pedestal rectangular end table	40
foldable pocket knife	14	Les Paul	67	pedestal round dining table	130	pedestal rectangular dinner table	38
dagger	12	Widow	55	simple rectangular coffee table	128	pedestal round coffee table	35
chef's knife	10	SG guitar	50	simple rectangular dining table	110	writing desk	32
throwing knife	9	Star	32	console table	100	office table	30
cleaver	8	Gibson Explorer	31	traditional rectangular dinner table	100	ping-pong table	29
dinner knife	8	cutaway	27	simple round end table	100	L-shape desk	28
karambit	7	Telecaster	21	simple round dining table	90	cross style round end table	24
dragon knife	6	Beast	16	modern rectangular coffee table	85	cabinet	20
		double-neck guitar	10	traditional rectangle coffee table	85	cross style round dining table	20
				office desk	80	cart	17
				simple round coffee table	77	hourglass round dining table	14
				training table	74	desk shell	12
				TV stand	67	secretaire	12
				multi-media table	64	hourglass round dinner table	12
				frame rectangular coffee table	57	lectern	9
				conference table	56	picnic table	8
				work bench	52	cross style round coffee table	8
				X-base rectangular dinner table	51		
Total	186		629				2607

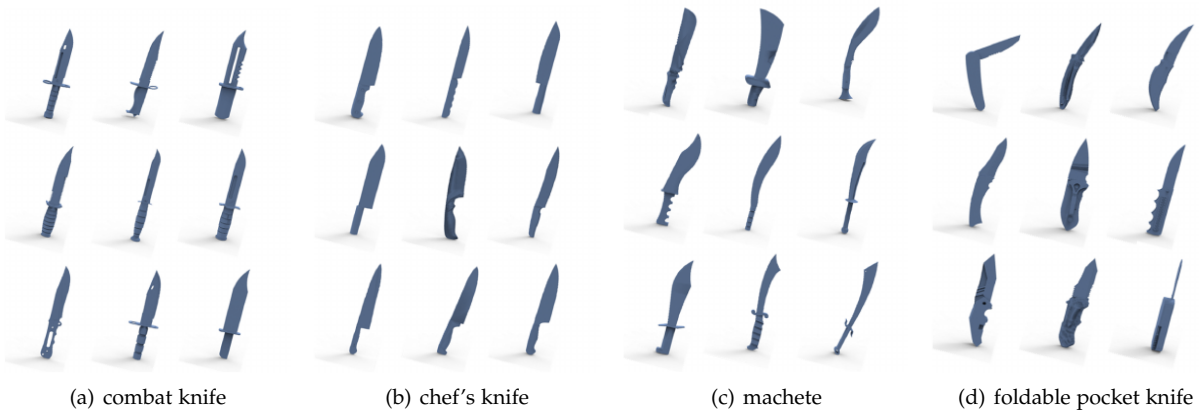


Fig. 16: Examples of four sub-classes under the knife category.

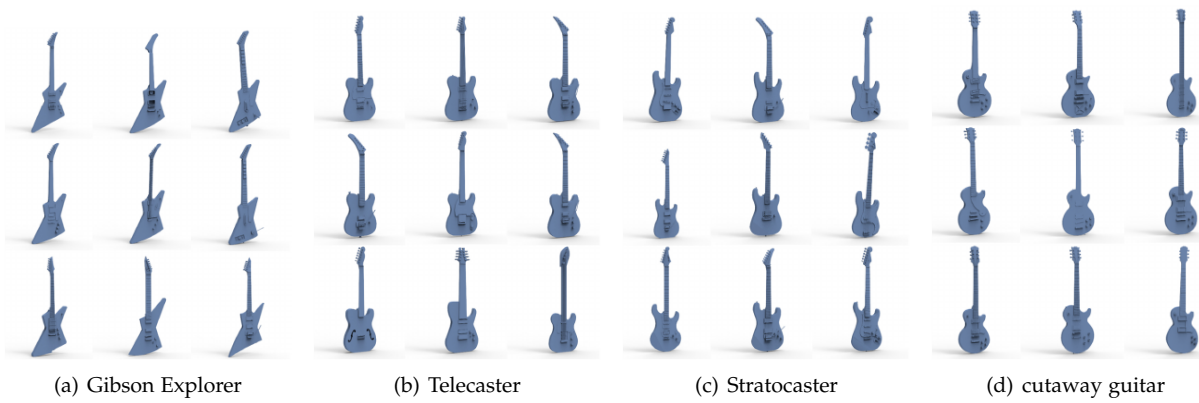


Fig. 17: Examples of four sub-classes under guitar category

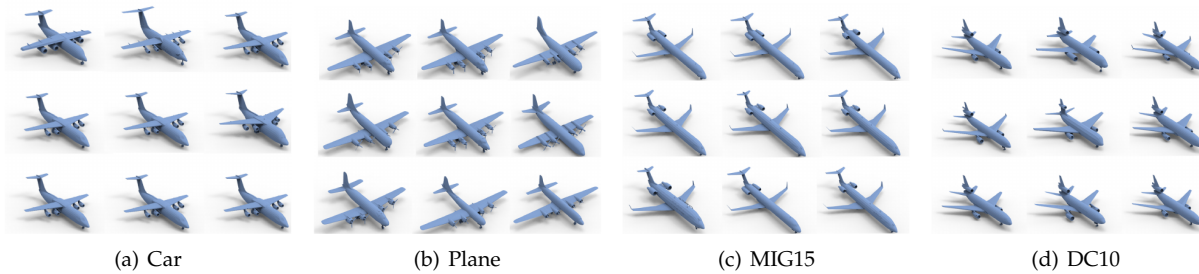


Fig. 18: Examples of four sub-classes under the plane category.

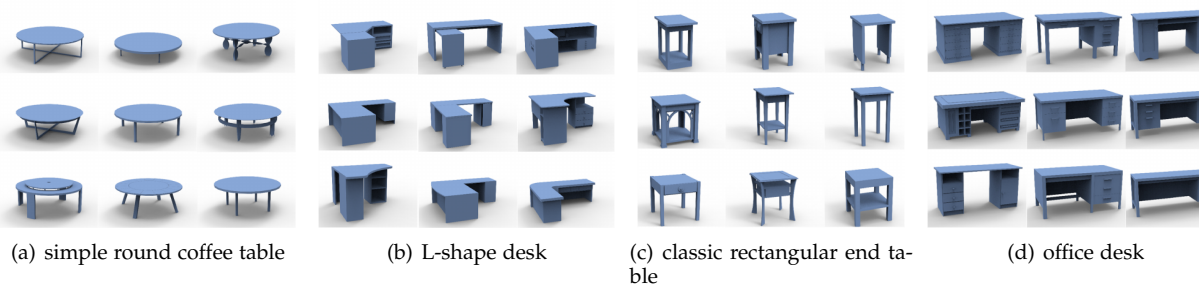
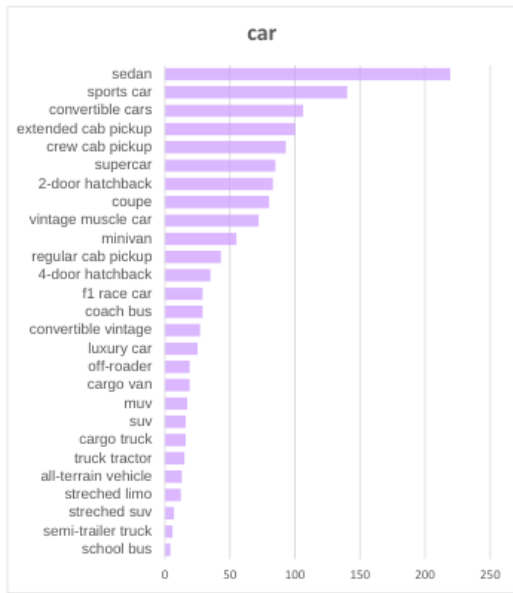
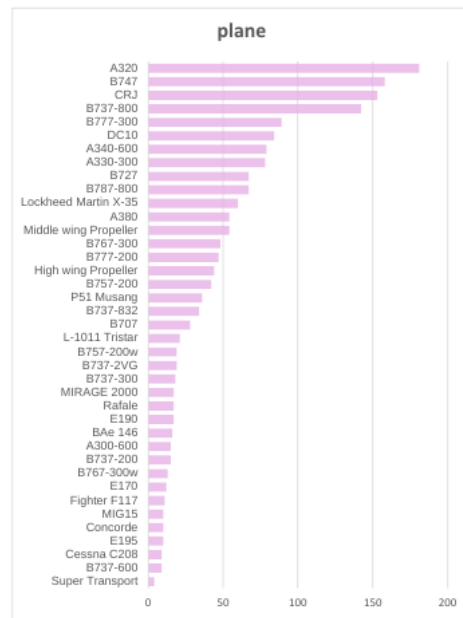


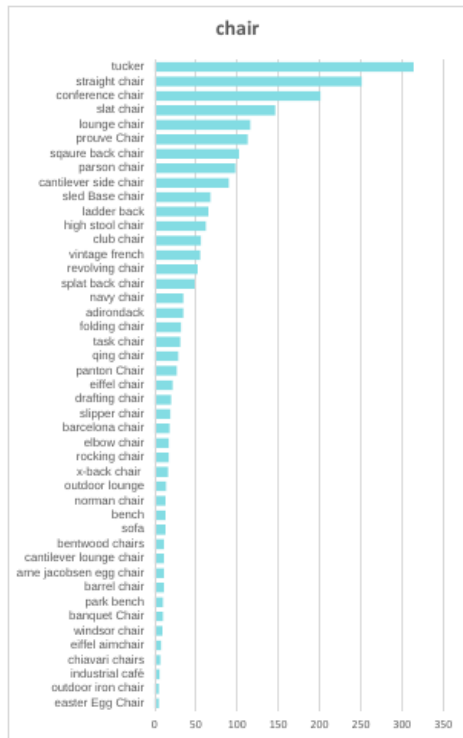
Fig. 19: Examples of four sub-classes under the table category.



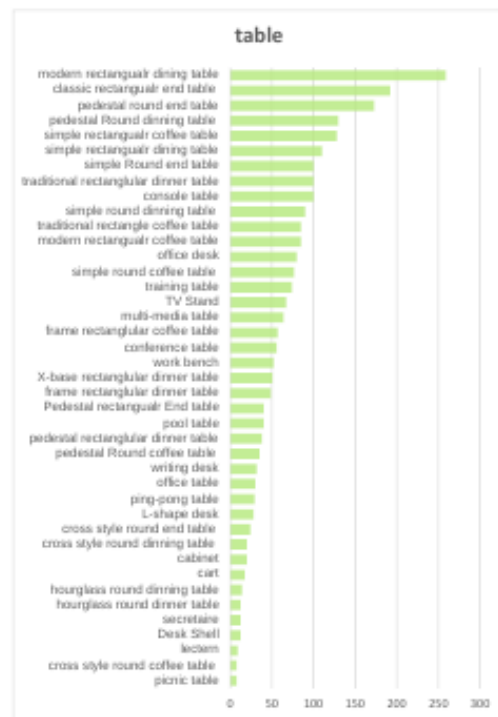
(a) car



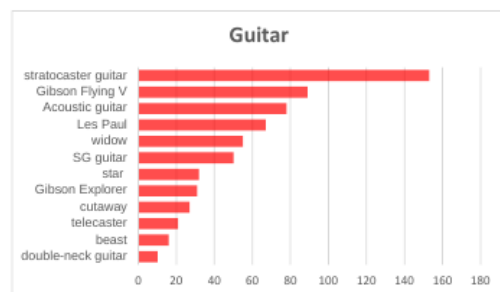
(b) plane



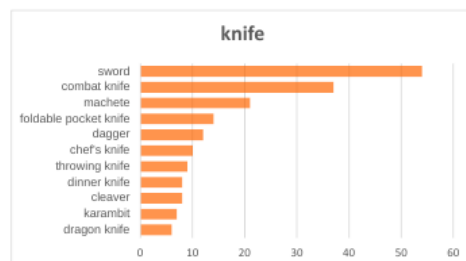
(c) chair



(d) table



(e) guitar



(f) knife

Fig. 20: Data Distribution

2 RETRIEVAL RESULTS

We use a shape repository containing both train and test set to evaluate its performance on large-scale dataset retrieval. In Table 7, we compare RISA-Net with other methods using five metrics on six object categories. RISA-net outperforms other methods on large-scale fine-grained shape retrieval.

We provide top-10 retrieval results when retrieving shapes from 6 object categories in our fine-grained 3D shape retrieval dataset. The query shape is from test set, and shape repository contains all shape of the same sub-class. The result shows that RISA-Net not only retrieves models with similar global structure, but also retrieves model with similar geometric features.

TABLE 7: Comparison between RISA-Net and other methods using five metrics on six object categories. The query shape is from test set, and shape repository contains all shape of the same sub-class.

Methods	micro					macro				
	NN	FT	ST	NDCG	mAP	NN	FT	ST	NDCG	mAP
SHD [7]	0.1983	0.1532	0.2749	0.5514	0.1529	0.1316	0.1013	0.1781	0.4604	0.1026
LFD [6]	0.2662	0.1947	0.3395	0.5835	0.1949	0.1717	0.1225	0.2147	0.4870	0.1263
MVCNN [14]	0.4346	0.1718	0.2754	0.5878	0.1635	0.3376	0.1246	0.1914	0.4995	0.1150
RotationNet [41]	0.1569	0.1371	0.2378	0.5304	0.1501	0.1274	0.1033	0.1687	0.4501	0.1146
Spherical [20]	0.2399	0.1301	0.2231	0.5353	0.1352	0.2233	0.1085	0.1807	0.4833	0.1044
SVSL [17]	0.3076	0.2309	0.3704	0.6134	0.2370	0.1955	0.1437	0.2372	0.5102	0.1508
MeshCNN [33]	0.4656	0.3070	0.4667	0.6681	0.3061	0.3453	0.2451	0.3824	0.5635	0.2519
Ours	0.7831	0.5651	0.6544	0.8101	0.5817	0.6908	0.4672	0.5401	0.7385	0.4817

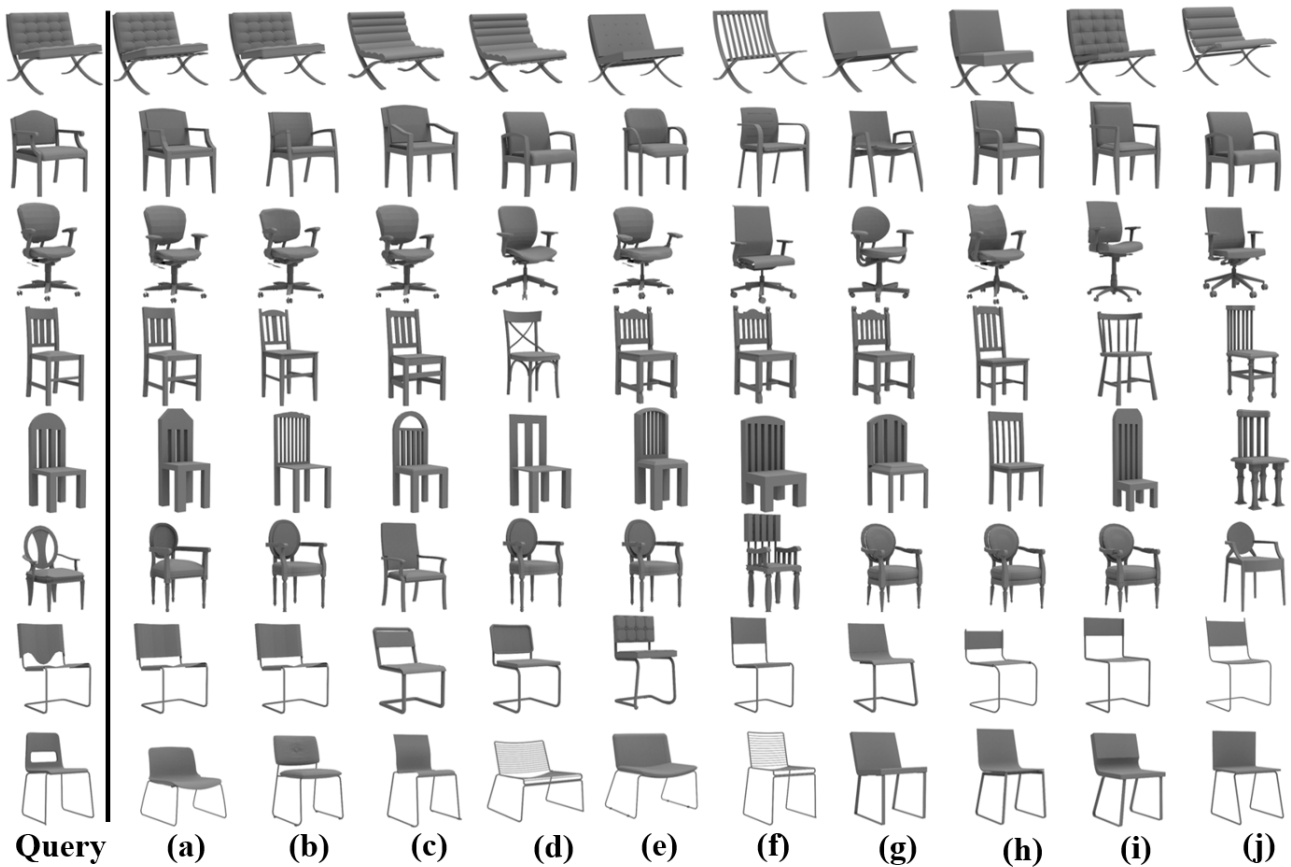


Fig. 21: Retrieval Results of Chairs

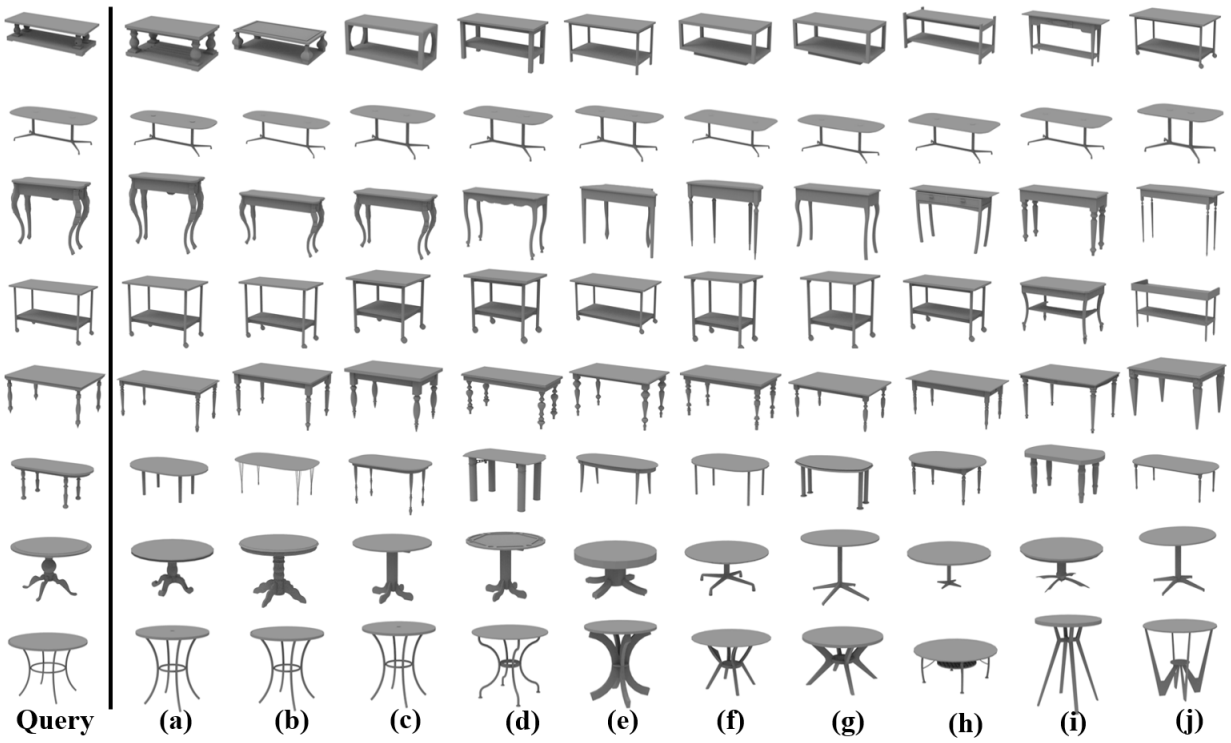


Fig. 22: Retrieval Results of Tables

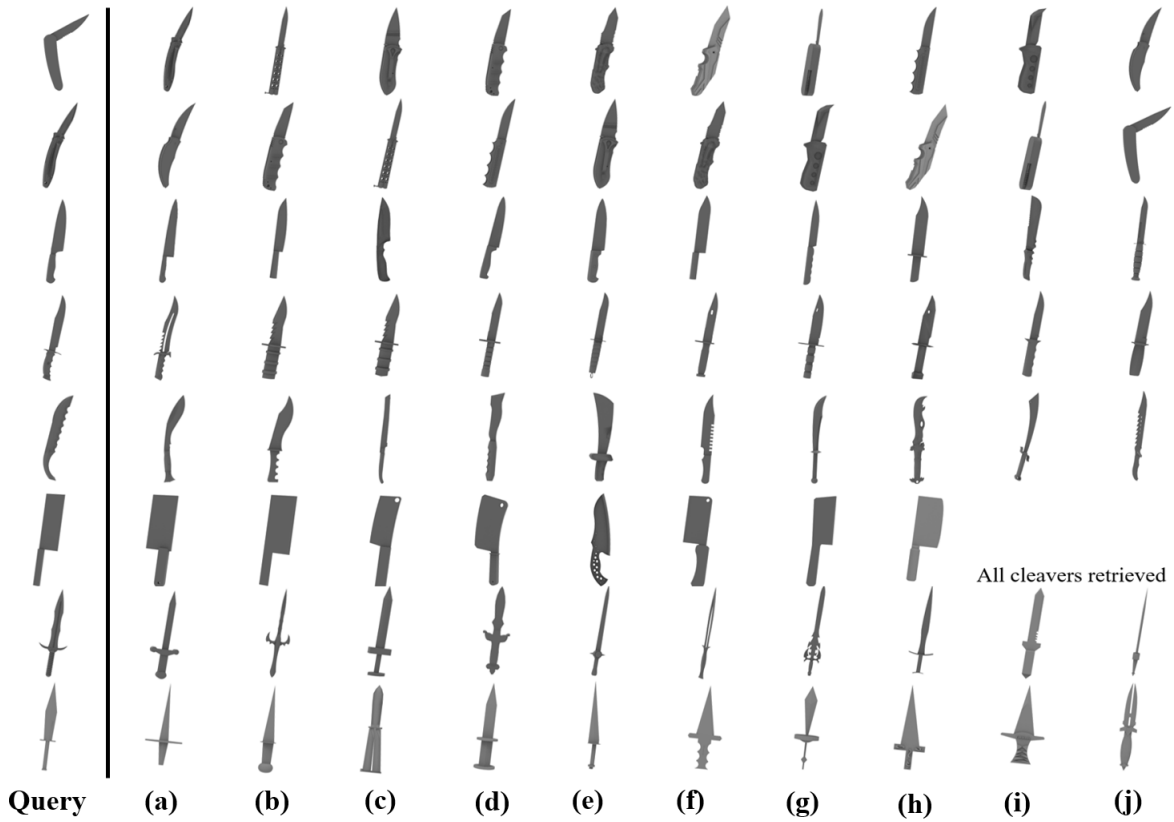


Fig. 23: Retrieval Results of Knives

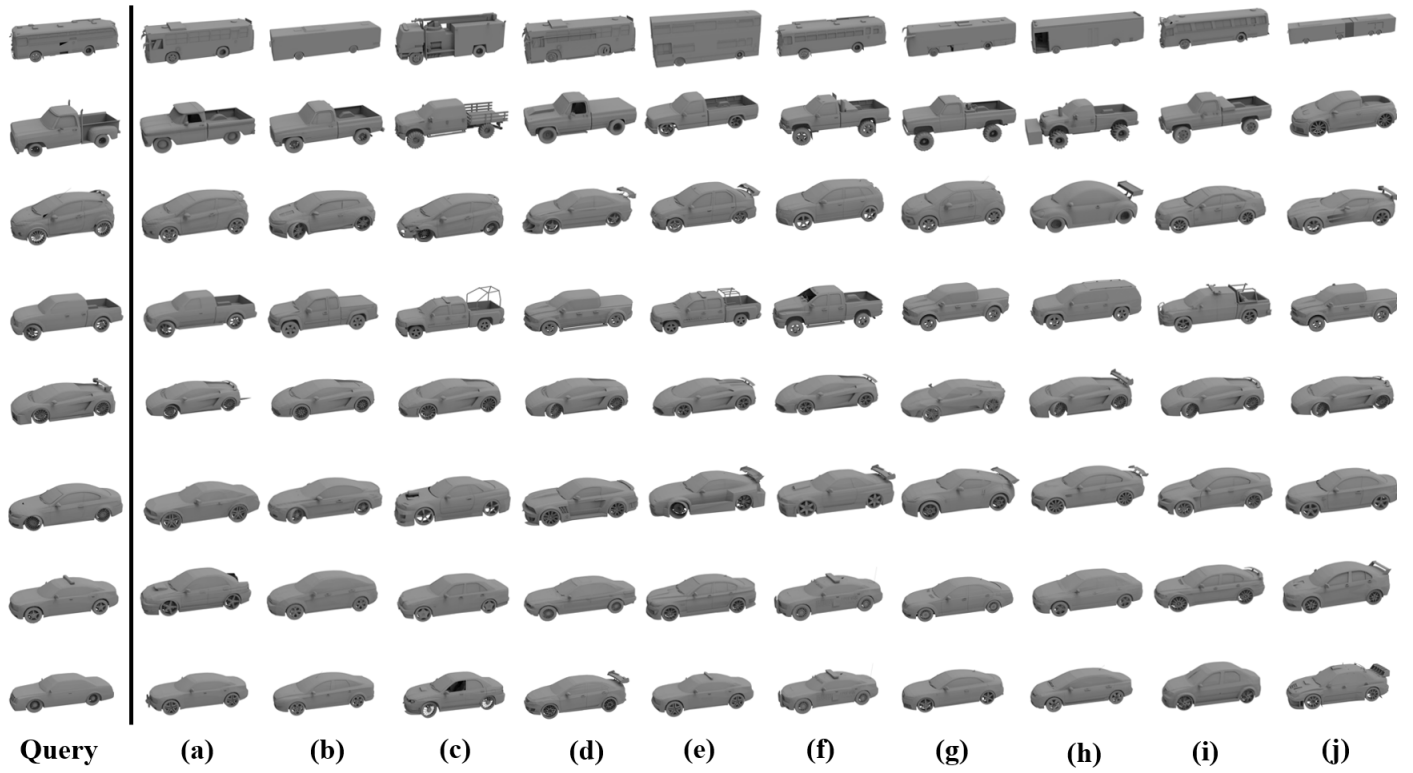


Fig. 24: Retrieval Results of Cars

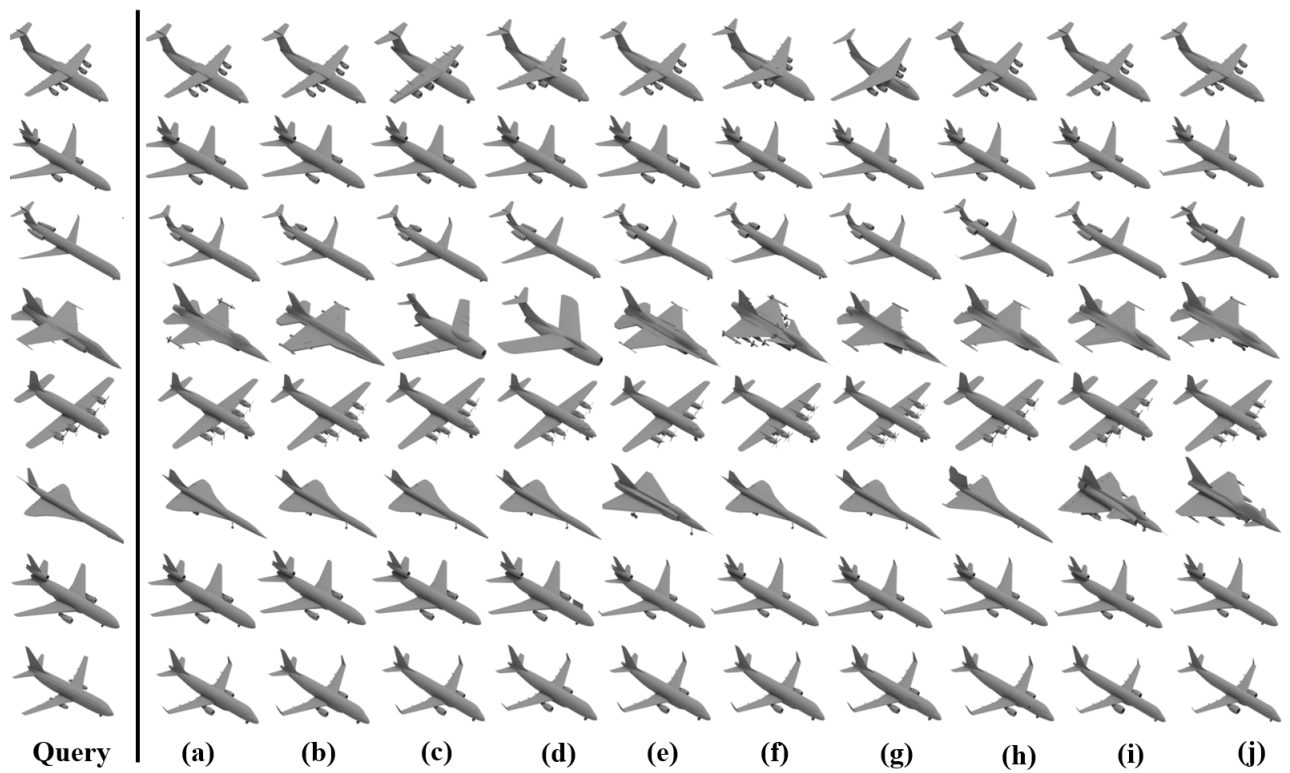


Fig. 25: Retrieval Results of Planes

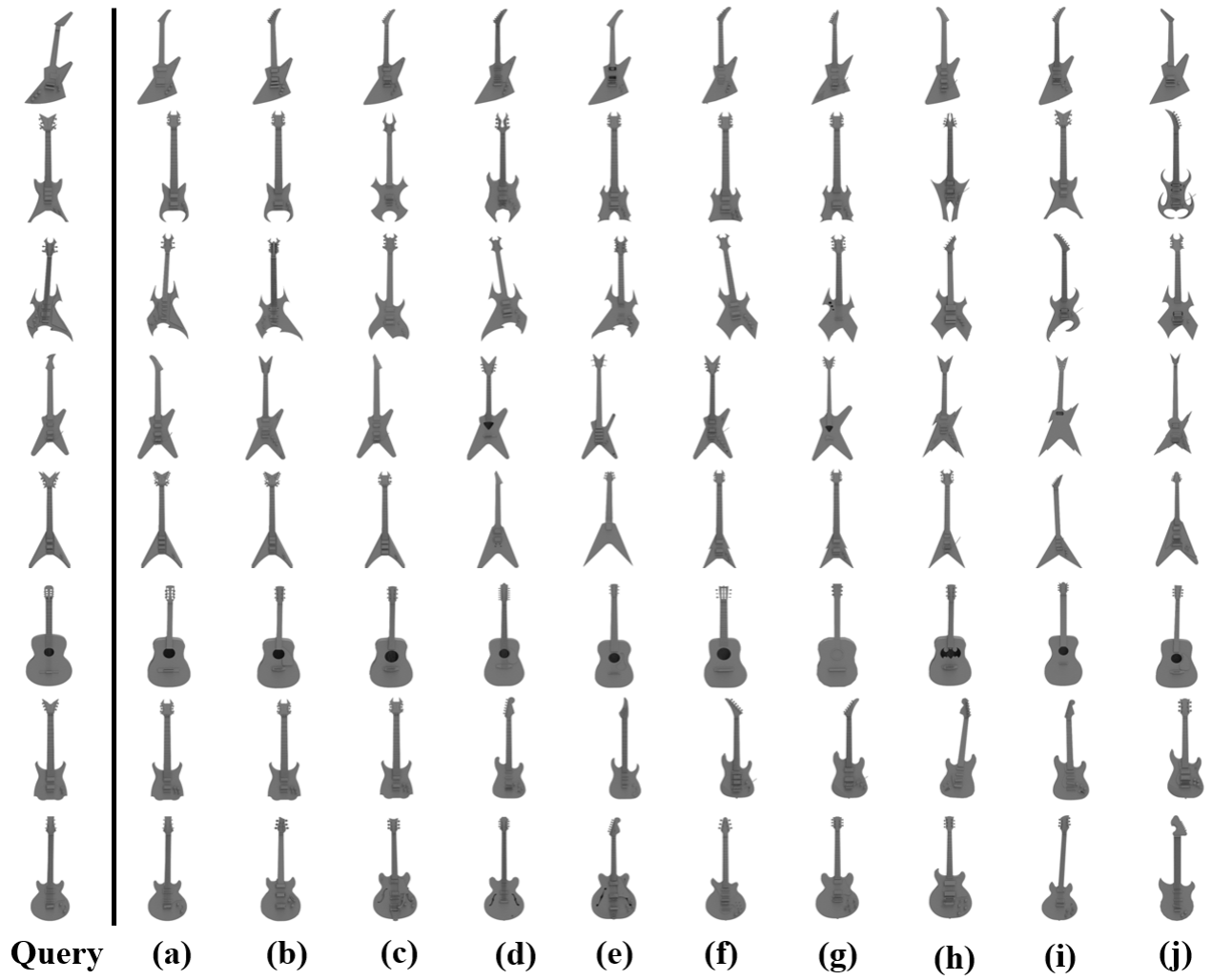


Fig. 26: Retrieval Results of Guitars